

Characterization of Longitudinal Neuroanatomical
Effects in a Mouse Model of Alzheimer's Disease
using Deformation-Based Morphometry

Jonathan C. Lau

Department of Biomedical Engineering
McGill University, Montréal
Québec, Canada

August 2008

A thesis submitted in partial fulfillment of the requirements of the
degree of Master of Engineering (Biomedical Engineering).

© Jonathan C. Lau, 2008

Abstract

While population analyses employing computational neuroanatomy have become common practice in magnetic resonance imaging (MRI) studies of human subjects, equivalent automated solutions for the study of mouse brain morphology have remained relatively unexplored. MRI studies of mice have largely been limited to labour-intensive, manual or semi-automated methods. In this thesis, the combined automated approaches of population-specific reference creation and deformation-based morphometry (DBM) were investigated in the context of a multiple timepoint study of a transgenic mouse model of Alzheimer’s disease and age-matched, wild-type littermates. Using a statistical framework based on mixed-model regression, the proposed technique provided an unbiased, exploratory summary of focal neuroanatomical differences due to genetic background, as well as localized regions exhibiting age-related change. Morphological abnormalities were found in the transgenic group in the hippocampus and ventricles, which are consistent with previous studies, as well as in several previously unreported structures such as the olfactory bulbs and stria terminalis. As validation, we found strong correlation between the results obtained using automated DBM analysis and conventional manual segmentation in specific neuroanatomical regions. Our findings suggest that DBM can be applied to the longitudinal study of other mouse models of central nervous system disease.

Résumé

Alors que l'analyse neuroanatomique quantitative des populations humaines est devenue courante en imagerie par résonance magnétique (IRM), de telles méthodes d'analyse automatisées sont essentiellement inexploitées pour l'étude des rongeurs. L'étude par IRM des souris repose ainsi principalement sur des méthodes manuelles ou semi-automatiques, impliquant une intervention lourde pour l'opérateur. Dans ce mémoire, une approche automatique est évaluée, qui combine la création d'un espace anatomique de référence spécifique de la population étudiée et l'analyse morphométrique des déformations (AMD, « deformation-based morphometry ») afin de comparer l'évolution de souris transgéniques, modèles de la maladie d'Alzheimer, avec un groupe de contrôle de la même portée. La technique proposée a su déceler sans biais des différences neuroanatomiques dues au bagage génétique en plus de localiser des régions sujettes à des changements liés au vieillissement à l'aide d'un modèle statistique de régression mixte. Les anomalies morphologiques ont été trouvées dans l'hippocampe et les ventricules de groupe transgénique, confirmant des résultats connus de la littérature, mais aussi dans de nouvelles régions, comme les bulbes olfactifs et la strie terminale. Comme validation de la méthode, nous avons mis en évidence une corrélation forte entre les résultats obtenus par AMD automatisée et par une méthode conventionnelle de segmentation manuelle de régions neuroanatomiques spécifiques. Ce travail démontre que des techniques de type AMD pourraient être appliquées à des études longitudinales de souris sur d'autres modèles de maladies du système nerveux central.

Acknowledgements

First of all, I would like to thank my co-supervisors, Dr. Alan Evans and Dr. Barry Bedell. I am grateful to Dr. Evans for bringing me here, providing an incredible environment for conducting brain research, and his inspiring vision of the BIC. I am indebted to Dr. Bedell for financial support and his active involvement in my project. His work ethic and multidisciplinary expertise have been motivating throughout this Master's project.

I am, of course, grateful to our collaborators from MICE (Dr. Jason Lerch, Dr. John Sled, and Dr. Mark Henkelman), and to Dr. Tomas Klason and Dr. Fu-Hua Wang from AstraZeneca R&D.

I would also like to thank my workmates, Pierre Bellec, Samir Das, Jürgen Germann, and Najma Khalili, who provided a stimulating office atmosphere open to discussing anything from neuroanatomy and statistics to life, politics, and basketball.

I owe a great deal to the community of MINC developers and users on whose tools my work is based. In particular, thanks must go to Louis Collins, Claude Lepage, Andrew Janke, and Vladimir Fonov. I am grateful to many others in the greater BIC community for their expertise and friendship: Reza Adalat, Antonio Aliaga, Sarah Assadian, Maxime Boucher, Mallar Chakravarty, Dale Einarson, Nicolas Guizard, Jonathan Harlap, Yong He, Kurt Hemmings, Ilana Leppert, Kelvin Mok, Sebastian Muehlboeck, Pedro Rosa-Neto, Beth Tannenbaum, Simone Zehntner, and Alex Zijdenbos.

Above all, I would like to thank my parents, Alison, and H el ene for their continued love, patience, and support.

Preface

In accordance with the McGill University Thesis Preparation and Submission Guidelines (Section I.C.), I have taken the option of writing a manuscript-based thesis. As such, the experimental portion of this Master's thesis has been included in the form of a paper published in *NeuroImage*, presented in Chapter 3. A common abstract, introduction, general literature review, summary, conclusions, and bibliography are included as required by the guidelines.

Contributions of Authors

For the original paper entitled “Longitudinal Neuroanatomical Changes Determined by Deformation-Based Morphometry in a Mouse Model of Alzheimer’s Disease” published in *NeuroImage* and included as part of the thesis, I (JCL) was the first author, with co-authors Drs. Jason P. Lerch (JPL), John G. Sled (JGS), R. Mark Henkelman (RMH), Alan C. Evans (ACE), and Barry J. Bedell (BJB). The project was supervised and funded by BJB and ACE. JPL, JGS, and RMH are collaborators from the MICe laboratory (Toronto, Ontario, Canada). The manuscript was written by JCL and BJB. Software for statistical analysis was developed by JPL. The image processing pipeline used in the study was developed by JPL and JCL. Longitudinal image processing and statistical analysis of the dataset were performed by JCL and JPL. Data management as well as pipeline evaluation and optimization were performed by JCL. JGS and RMH are the senior collaborative authors from the MICe laboratory, who developed the reference creation software used in the study (see Kovacevic et al., 2005). BJB and ACE are the senior corresponding authors on the manuscript and abstracts written throughout the course of the Master’s project, and for the tools used in this analysis.

The authors would also like to acknowledge Drs. Tomas Klason and Fu-Hua Wang at the MR Center of AstraZeneca R&D (AstraZeneca, Södertälje, Sweden) for kindly supplying the MRI and manual segmentation datasets.

Contents

Abstract	i
Résumé	ii
Acknowledgements	iii
Preface	iv
Contributions of Authors	v
List of Figures	viii
List of Tables	x
List of Abbreviations	xi
1 Introduction	1
1.1 Research objectives	3
1.2 Thesis organization	3
2 Literature Review	4
2.1 Alzheimer’s disease	4
2.1.1 Clinical findings	4
2.1.2 Pathological staging	7
2.1.3 Management	8
2.1.4 Genetic determinants and risk factors	8
2.1.5 Mouse models of AD	9
2.2 Magnetic resonance imaging	11
2.3 Manual Segmentation	13
2.4 Computational neuroanatomy	14
2.4.1 Atlas-based segmentation methods	14
2.4.2 Tissue classification methods	16
2.4.3 Deformation-based morphometry	17
2.5 Longitudinal analysis	20
2.6 Research justification	21

3	Manuscript for <i>NeuroImage</i>	24
3.1	Abstract	25
3.2	Introduction	25
3.3	Materials and methods	27
3.3.1	Animals and MRI measurements	27
3.3.2	Longitudinal deformation-based morphometry	28
3.3.3	Longitudinal statistical analysis of the voxelwise Jacobian	31
3.3.4	Relationship between DBM results and conventional manual volumetry	32
3.4	Results	33
3.4.1	Reference model and nonlinear registration	33
3.4.2	Results of longitudinal DBM analysis	33
3.4.3	Longitudinal findings from manual segmentations	34
3.4.4	Correlation between automated and manually segmented measures	35
3.5	Discussion	35
3.6	Acknowledgements	39
4	Summary of Findings	49
5	Conclusions	51
6	Future Work	52
	Bibliography	54

List of Figures

2.1	The estimated number of individuals in the United States with AD projected from data from the 2000 US Census Bureau to the year 2050 (Hebert et al., 2003). The middle series estimate is bounded by lower and upper estimates.	5
2.2	Clock drawings and associated Mini-Mental State Examination scores for four individuals. Patients were all instructed to write the time as "10 minutes past 11" (Feldman et al., 2008).	6
2.3	The distribution pattern of amyloid deposits, which is shown to originate in the basal part of the isocortex, and eventually spread to all cortical regions (Braak and Braak, 1991).	7
2.4	The distribution pattern of neurofibrillary tangle formation, which originates focally in the transentorhinal region, and eventually involves more regions of the isocortex (Braak and Braak, 1991).	8
2.5	The distribution pattern of amyloid deposits shown for the APP/PS1 mouse at (A) 6, (B) 9, (C) 12, and (D) 15 months of age (th = thalamus, hc = hippocampus, s = striatum, fcx = frontal cortex) (Gordon et al., 2002).	10
2.6	Example slices from a human T ₁ -weighted image (a-c), and a mouse T ₂ -weighted image (d-f) in the three standard viewing planes. In a T ₁ -weighted image, GM appears gray, CSF appears dark, and WM appears white. In a T ₂ -weighted image, GM appears gray, CSF appears white, and WM appears dark. Indicators are included for the various tissue types. WM* indicates a region where WM is expected but cannot be resolved at the acquired resolution. Note the obvious difference in cortical complexity of the human and mouse brains. . . .	12
2.7	Manual volumes for (a) whole brain, (b) hippocampus, and (c) ventricles in TG and WT mice across three timepoints. Volume is reduced in whole brain and hippocampus measures in tg, and increased in the ventricular volume (Oberg et al., 2007) (tg = APP/PS1; wt = wild-type).	13
2.8	Illustration of the unbiased reference creation image processing pipeline described by Kovacevic et al. (Kovacevic et al., 2002). The pipeline uses tools developed at the Brain Imaging Centre that have been made freely available to the neuroimaging community.	19

3.1	Pipeline results for successive stages of reference creation. (a) Average and standard deviation images of the same transverse slice at successive stages of registration. (b) Plots of performance (quantified as voxel overlap) versus registration step for each manually segmented scan. Note that the performance of the algorithm is seen to plateau after the sixth nonlinear registration step.	43
3.2	Statistical maps demonstrating local volume differences between TG and WT populations. (a) The positions of representative slices throughout the reference space are marked with dashed lines in a mid-sagittal slice for the coronal sections (A-E) and a mid-transverse slice for the sagittal sections (F-J). (b) Regions demonstrating volumetric differences due to genotype across all timepoints. Volumetric expansion and reduction in TG versus WT are shown in green and red, respectively. (c) Regions demonstrating dynamic interactions between age and genotype. Positive and negative interactions are shown in green and red, respectively. All coloured regions are statistically significant by pooled FDR ($q = 0.05$).	44
3.3	Dynamic longitudinal changes illustrated within the hippocampus using the local scaled Jacobian. The voxelwise scaled Jacobians are plotted as open circles. The final predicted model, represented by a thick solid line, includes only significant components of the mixed-effects model, and individual trajectories are connected by thin solid lines. Regions in (a) the left lateral dentate gyrus, (b) the right dorsal hippocampus within CA1, and (c) the left dorsal hippocampal commissure are shown.	45
3.4	Dynamic longitudinal changes illustrated for several regions throughout the brain. The voxelwise scaled Jacobians are plotted as open circles. The final predicted model, represented by a thick solid line, includes only significant components of the mixed-effects model, and individual trajectories are connected by thin solid lines. Regions of (a) the left lateral entorhinal cortex, (b) the lateral ventricles, and (c) the bed nucleus of the stria terminalis are shown.	46
3.5	Mixed-effects regression plots in three manually segmented neuroanatomical volumes: (a) whole brain, (b) hippocampus, and (c) lateral ventricles. The raw datapoints are plotted as open circles. The final predicted curve is represented by a solid line, and individual trajectories are connected by thin solid lines.	47
3.6	Correlation between automated and conventional manual segmentations of (a) whole brain, (b) hippocampus, and (c) lateral ventricles. .	48

List of Tables

3.1	Registration schedule	40
3.2	Main effects of genotype	41
3.3	Interactions between age and genotype	42

List of Abbreviations

2D:	Two-dimensional
3D:	Three-dimensional
4D:	Four-dimensional
AD:	Alzheimer's disease
APoE4:	Apolipoprotein E (allele 4)
APP:	Amyloid-precursor protein
CNS:	Central nervous system
CSF:	Cerebrospinal fluid
DBM:	Deformation-based morphometry
DNA:	Deoxyribonucleic acid
FAD:	Familial Alzheimer's disease
fMRI:	Functional magnetic resonance imaging
FOV:	Field of view
FWHM:	Full width at half maximum
GM:	Gray matter
LOAD:	Late-onset Alzheimer's disease
MRI:	Magnetic resonance imaging
NEX:	Number of excitations
PET:	Positron emission tomography
PS1:	Presenilin 1
RARE:	Rapid acquisition with relaxation enhancement
ROI:	Region of interest
SORL1:	Sortilin-related receptor 1
SNR:	Signal-to-noise ratio
TE:	Echo time
TG:	Transgenic
TR:	Repetition time
WM:	White matter
WT:	Wild-type
VBM:	Voxel-based morphometry

Chapter 1

Introduction

Alzheimer's disease (AD) is the leading cause of senile dementia with prevalence expected to increase markedly in the next few decades (Hebert et al., 2003). While researchers have revealed specific genetic and social factors associated with AD onset (reviewed by Selkoe, 2001), the etiology of the disease remains poorly understood. As the search for effective therapies continues, the role of transgenic mouse models of AD has become increasingly important for the identification of molecular targets involved in AD pathogenesis (reviewed by Higgins and Jacobsen, 2003). Typically, studies of transgenic mouse models have employed classical immunohistochemistry techniques (Higgins and Jacobsen, 2003), as well as behavioural assessment (Holcomb et al., 1999; Howlett et al., 2004; Trinchese et al., 2004) to evaluate and detect genotype-related abnormalities.

Magnetic resonance imaging (MRI) has become an invaluable tool for the non-invasive detection of abnormal morphological patterns in neurological disorders. While computational neuroanatomy approaches are commonly used in both cross-sectional and longitudinal imaging studies of human AD subjects (reviewed by Anderson et al., 2005; Barnes et al., 2007; Thompson et al., 2007), equivalent automated solutions for the study of mouse neuroanatomy have remained largely unexplored. Most MRI studies of AD mouse models have used labour-intensive manual or semi-automated techniques to examine differences in the volume of structures between normal and transgenic mice (Redwine et al., 2003; Delatour et al., 2006; Oberg et al., 2007). There are few impediments to the translation of fully-automated techniques used in

human imaging studies to the analysis of murine brain MRI. This thesis serves to investigate computational neuroanatomy methods for characterizing mouse models of AD, with particular application to a longitudinal MRI dataset of double transgenic APP/PS1 (TG) mice and their age-matched, wild-type (WT) littermates.

Automated image processing techniques, such as atlas-based segmentation, voxel-based morphometry (VBM), and cortical thickness analysis, are powerful approaches that have the potential to all be used for the analysis of mouse MRI data. However, these methods require *a priori* information about anatomical labels and tissue classes, for which a number of digital mouse atlases have been proposed (Dhenain et al., 2001; MacKenzie-Graham et al., 2004; Ma et al., 2005; Kovacevic et al., 2005; Schwarz et al., 2006). These atlases are also not often scanned in modalities or using methods compatible across sites or laboratories, suggesting that other more data-driven options be explored.

Deformation-based morphometry (DBM) is an established, automated method that can detect localized, morphological differences from the vector field required to nonlinearly register MR images (Davatzikos et al., 1996; Bookstein, 1997; Thompson and Toga, 1997; Ashburner et al., 1998; Cao and Worsley, 1999; Chung et al., 2001). This technique has recently been applied to study normal (Kovacevic et al., 2005; Chen et al., 2006; Spring et al., 2007) and transgenic mice (Nieman et al., 2005a). Aside from the chosen reference space to which all original data are registered, DBM requires no prior information other than the input MR images. The DBM approach also has the advantage of being exploratory in nature and is capable of providing more focal information about neuroanatomically-affected regions than conventional manual segmentation methods.

While DBM is now commonly used for exploratory brain MR analysis, the use of DBM to analyze longitudinal data has not been thoroughly investigated. Both human and mouse neuroimaging studies using automated DBM have mainly been limited to cross-sectional or two timepoint observations. While Verma et al. have utilized DBM for more timepoints in studies of murine development (Verma et al., 2005; Zhang et al., 2005), their method relied on semi-automated registration and did not address the issue of performing a unified analysis in a common reference space.

1.1 Research objectives

In this thesis, DBM is investigated as an automated technique for examining local neuroanatomy in a longitudinal MRI dataset of TG and WT mice. The research objectives are the following:

1. Develop a pipeline framework for image analysis of rodent models
2. In a mouse model of Alzheimer’s disease, characterize:
 - Morphological changes over time
 - Morphological differences due to genetic background

1.2 Thesis organization

The thesis is structured in the form of a manuscript-based thesis in accordance with McGill University Thesis Guidelines. Chapter 2 is a review of literature, starting with a synopsis of AD-related research, and followed by a summary of emerging techniques for studying Alzheimer’s, namely: transgenic technology, magnetic resonance imaging, and computational neuroanatomy. Chapter 3 contains the manuscript entitled “Longitudinal Neuroanatomical Changes Determined by Deformation-Based Morphometry in a Mouse Model of Alzheimers Disease” published in *NeuroImage*. This chapter is followed by a summary of the work, conclusions, and future work sections in Chapters 4, 5, and 6, respectively.

Chapter 2

Literature Review

2.1 Alzheimer's disease

Alzheimer's disease (AD) is a devastating, neurodegenerative disease with prevalence expected to increase substantially over the next few decades (Figure 2.1) (Hebert et al., 2003). The progressive, protracted decline of cognitive function and behaviour in AD patients places major emotional, physical, and financial burdens on families and the healthcare providers that support them (Mount and Downton, 2006). Despite having been first identified in 1901 by Dr. Alois Alzheimer, there remains no effective treatment for the disease, as currently available drugs have only limited, short-term effects. The increasing prevalence and lack of therapeutic options indicate an urgent need to improve understanding of disease pathogenesis, and to develop novel avenues for the prevention and treatment of AD.

2.1.1 Clinical findings

AD is characterized by a typically gradual and progressive course affecting cognitive abilities. Common early to moderate stage clinical features include memory loss, disorientation, depression, and difficulties with judgement, language, and calculations. Evidence suggests that mild cognitive impairment (MCI), a clinical syndrome marked

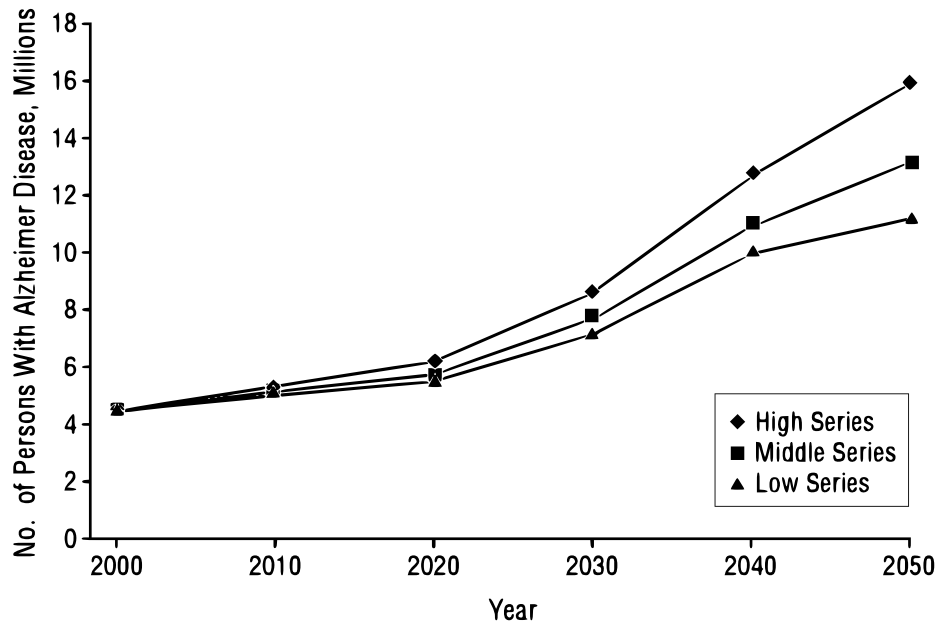


Figure 2.1: The estimated number of individuals in the United States with AD projected from data from the 2000 US Census Bureau to the year 2050 (Hebert et al., 2003). The middle series estimate is bounded by lower and upper estimates.

by both subjective and objective measures of memory loss, significantly increases the risk of progression to AD (Singh et al., 2006). AD patients may additionally exhibit behavioural changes and difficulties performing learned motor tasks. Ultimately, the patient’s function will decline to a point where the patient requires total care for all activities of daily living. Sporadic AD, the most common form of the disease, does not typically present until the age of 60, and while heterogeneous, the rate of progression has been estimated to take between 5 and 15 years to advanced stage illness (Andreoli et al., 2007).

Diagnosis involves establishing features of dementia on examination and the exclusion of other non-cognitive illnesses. The Mini-Mental State Examination (MMSE), a standardized neuropsychological test, provides a measure of the degree of functional decline by quantifying attention/concentration, memory/orientation, learning, and language deficits (Folstein et al., 1975). The clock drawing test is another useful procedure for assessing the degree of cognitive dysfunction (Freedman et al., 1994) (Figure 2.2). These tests can be used to distinguish AD from other types of dementia.

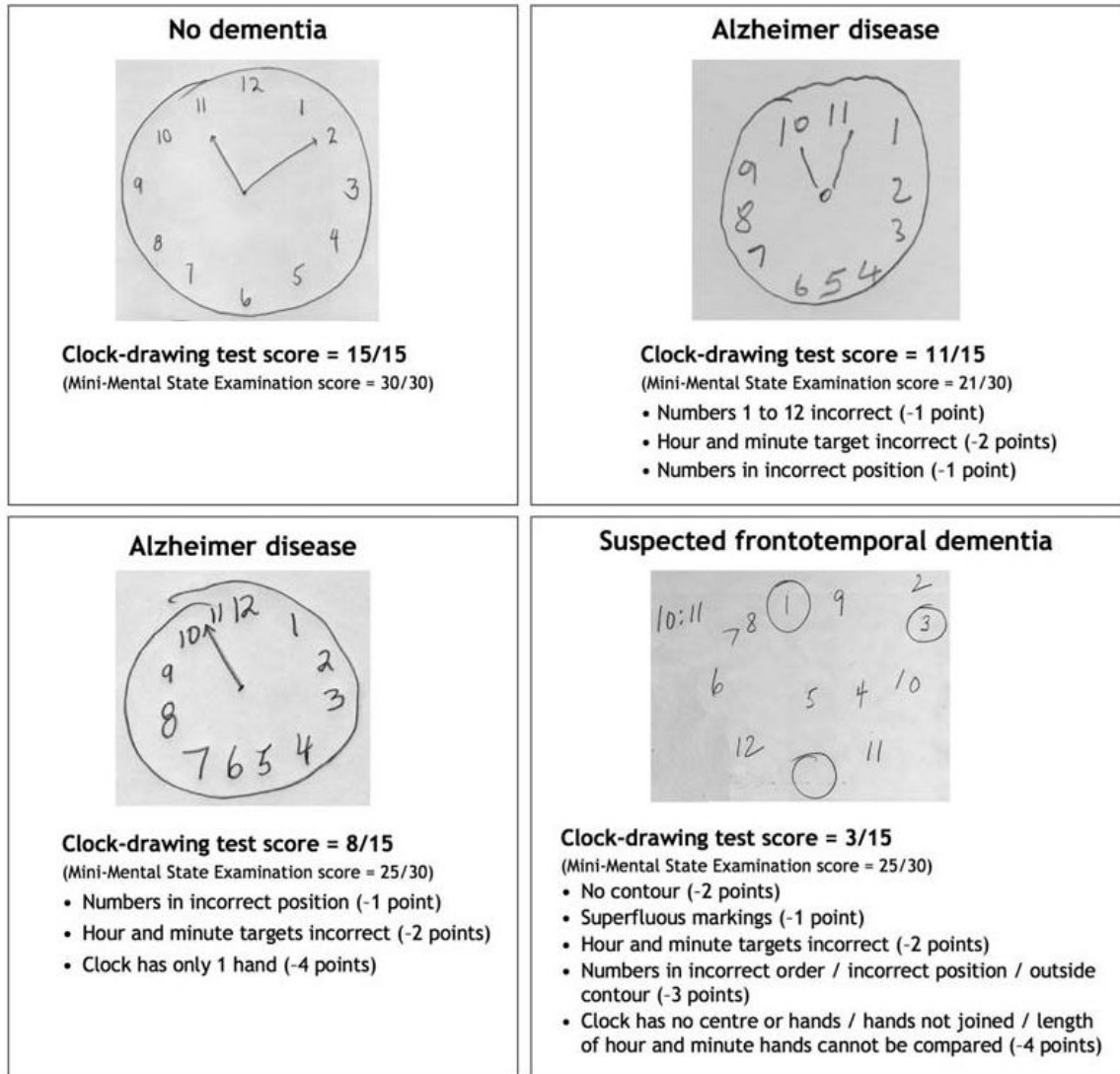


Figure 2.2: Clock drawings and associated Mini-Mental State Examination scores for four individuals. Patients were all instructed to write the time as "10 minutes past 11" (Feldman et al., 2008).

2.1.2 Pathological staging

In humans, classical histochemistry and immunohistochemistry approaches have identified several major neuropathological features of AD. This disease is characterized by the formation of extracellular neuritic plaques, as well as intracellular neurofibrillary tangles (Selkoe, 2001). In studies of affected brains at autopsy, Braak and colleagues observed that both the distribution of β -amyloid plaque deposition and neurofibrillary tangles exhibited differential staging depending on the severity of disease (Braak and Braak, 1991; Thal et al., 2002). Plaque deposition was observed to begin in the medial temporal neocortex before expanding into other neocortical and allocortical regions (Figure 2.3), while tangle formation was found to originate in the transentorhinal and entorhinal cortices prior to affecting other regions of the cortex (Figure 2.4).

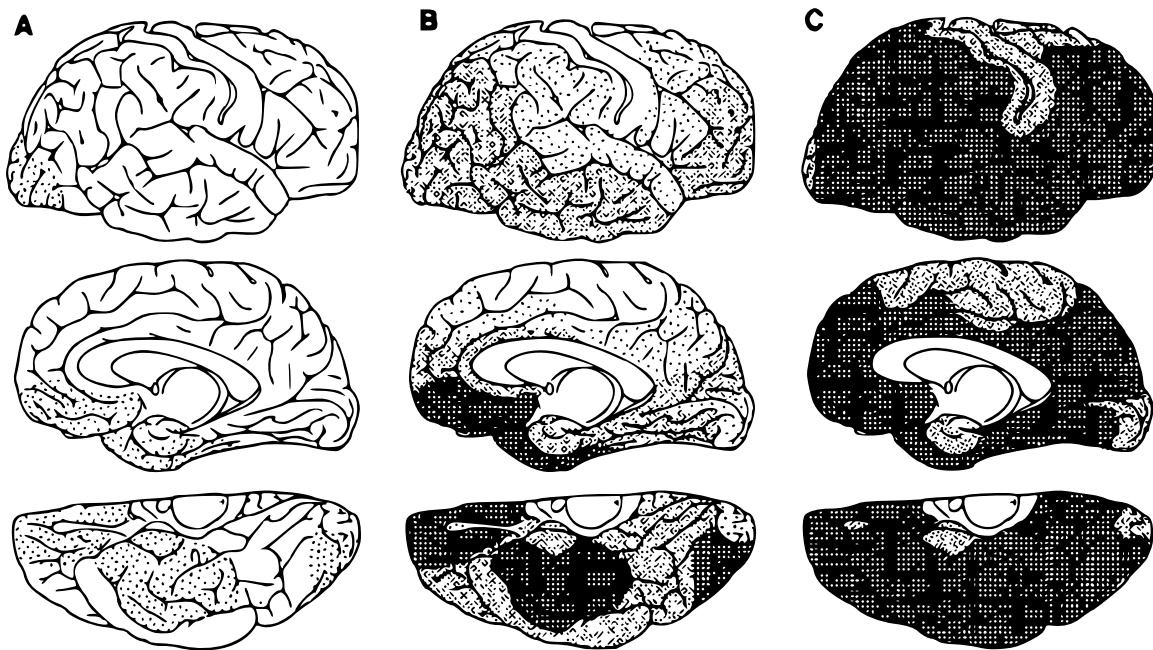


Figure 2.3: The distribution pattern of amyloid deposits, which is shown to originate in the basal part of the isocortex, and eventually spread to all cortical regions (Braak and Braak, 1991).

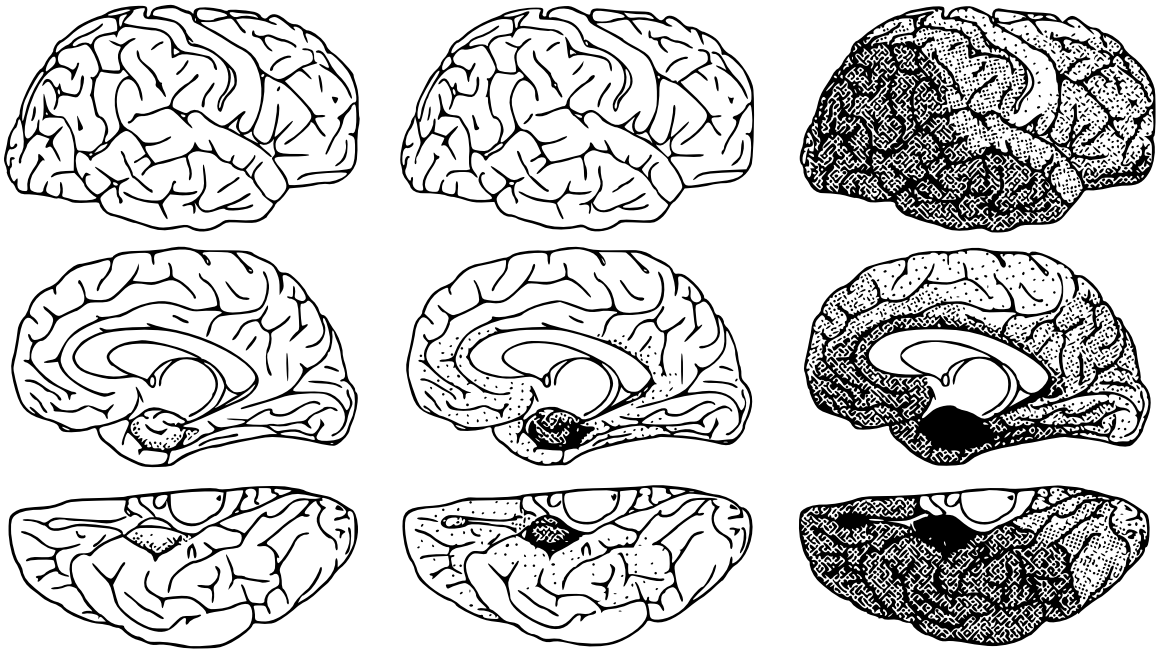


Figure 2.4: The distribution pattern of neurofibrillary tangle formation, which originates focally in the transentorhinal region, and eventually involves more regions of the isocortex (Braak and Braak, 1991).

2.1.3 Management

Current therapies of AD are non-curative, and are aimed at slowing the progression of degeneration (Doody et al., 2001). The use of cholinesterase inhibitors is considered standard practice for patients with mild to moderate disease due to some demonstrated efficacy for improving cognition and behaviour. Memantine, an NMDA receptor antagonist, has been shown to prolong daily functioning in patients with moderate to severe AD. Antidepressants, antipsychotics, and anxiolytics have been used to treat coexistent depression or acute behavioural disturbances as appropriate.

2.1.4 Genetic determinants and risk factors

Studies have revealed several hereditary components of AD. In particular, studies in humans have identified three autosomally dominant traits genetically linked with early-onset familial AD (FAD): amyloid precursor protein (APP) (Goate et al., 1991;

Mullan et al., 1992), presenilin 1 (PS1) (Schellenberg et al., 1992), and presenilin 2 (PS2) (Levy-Lahad et al., 1995; Sherrington et al., 1995). Even though, FAD accounts for less than 5% of all cases of AD in humans, research into these rare and severe forms of the disease have helped identify some of the key mechanisms involved in the disease cascade. In particular, mutations in APP, PS1, and PS2 have all been found to contribute to disordered β -amyloid metabolism (Selkoe, 2001; Jack et al., 2007). Population studies of the more prevalent sporadic, or late-onset AD (LOAD), form have revealed that mutations in two additional genes have been identified as potential risk factors: allele 4 of apolipoprotein E (ApoE4) (Corder et al., 1993) and sortilin-related receptor (SORL1) (Rogaeva et al., 2007). These components may serve as potential therapeutic targets for treating AD.

2.1.5 Mouse models of AD

With the development of recombinant DNA technology, researchers are now able to examine the effects of mutations in disease-related genes on transgenic animals, typically in mice. Transgenic mice are the product of a process that involves inserting target genes of interest, or *transgenes*, into the mouse genome, and provide simplified biosystems for examining the pathogenesis of disease (Hsiao et al., 1996; Holcomb et al., 1998; Games et al., 2006). Modified or novel traits observed in the genetically modified mice, in pathology or behaviour, indicate phenotypic abnormalities that may be worthy of further study. Their role has become increasingly important in the identification of molecular targets involved in AD pathogenesis, and a wide variety of mouse models have been proposed, developed, and subsequently investigated (reviewed by Higgins and Jacobsen, 2003).

The double transgenic APP/PS1 mouse

In this thesis, the double transgenic APP/PS1 (TG) mouse, which co-expresses mutations in both APP and PS1 transgenes, was investigated. This commonly studied AD mouse model has been reported to exhibit accelerated plaque pathology, beginning as early as 2 months of age (Borchelt et al., 1997; McGowan et al., 1999; Kurt et al., 2001; Gordon et al., 2002; Delatour et al., 2006; Oberg et al., 2007).

While APP/PS1 mice do not exhibit tangle pathology, the relatively early-onset of β -amyloid deposits makes this mouse an ideal candidate for evaluating the effects of β -amyloid targeted therapies (Figure 2.5). Beyond amyloidogenesis, evidence of progressive synaptic dysfunction (Trinchese et al., 2004), impairment of hippocampal neurogenesis (Zhang et al., 2006), and cognitive deficit in behavioural tasks (Holcomb et al., 1999; Gordon et al., 2001; Howlett et al., 2004) have been observed to advance with age in this transgenic model, typically occurring by 9–10 months of age.

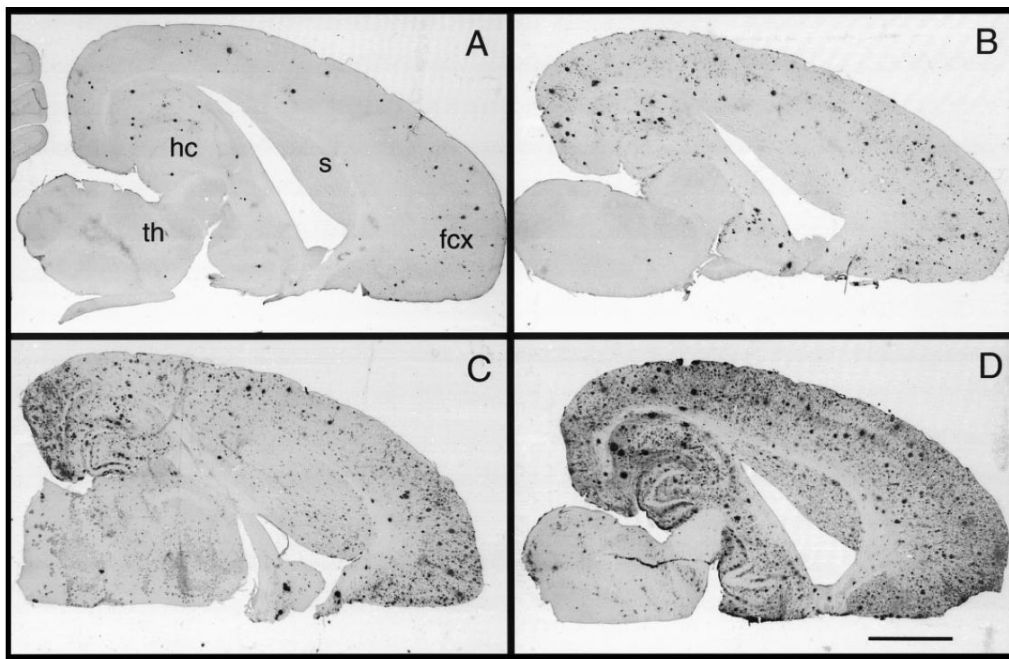


Figure 2.5: The distribution pattern of amyloid deposits shown for the APP/PS1 mouse at (A) 6, (B) 9, (C) 12, and (D) 15 months of age (th = thalamus, hc = hippocampus, s = striatum, fcx = frontal cortex) (Gordon et al., 2002).

Most studies of APP/PS1 and other transgenic mouse models have employed immunohistochemistry, as well as behavioural assessment, to evaluate and characterize abnormal phenotypes. While immunohistochemistry remains the standard for assessing microstructural and pathological effects, clearly less invasive means of studying structural abnormalities are worthy of investigation. On the other hand, behavioural studies may be necessary for elucidating task-related aberrations, but on their own, provide little information about the anatomical underpinnings of dysfunction. Magnetic resonance imaging techniques provide an alternative, and complementary, modality for assessing and characterizing mouse models of AD.

2.2 Magnetic resonance imaging

Magnetic resonance imaging (MRI) has become an invaluable diagnostic tool for the non-invasive, three-dimensional (3D) imaging of biological tissues. The principles of MR, also known more precisely as *nuclear* MR (NMR), are based on the interaction of the nuclear spin angular momentum of atoms with different magnetic fields. While a broad range of nuclei can be imaged with MRI, proton MRI is the most common form due to the natural abundance of H₂O in the body. Image contrast is optimized by exploiting differences in magnetic properties of tissues of interest (more specifically, T₁ and T₂ relaxation properties), which in the brain are principally gray matter (GM), white matter (WM), and cerebrospinal fluid (CSF).

Different techniques have been developed to take advantage of different aspects of magnetic resonance and tissue properties. These include functional magnetic resonance imaging (fMRI), where changes in regional blood-oxygenation level dependency (BOLD) are believed to be associated with local functional brain activation, as well as magnetic resonance spectroscopy (MRS), where local biochemical information can be elucidated in brain regions of interest. Here we focus on anatomical or structural MRI, which is used to visualize the neuroanatomy of the brain. Anatomical MR images are composed of individual “volume elements” called *voxels*. The resolution provides a measure of the level of detail in an image quantified spatially as the dimensions of the voxels in the image. Typical clinical MRI resolution is around 1 mm × 1 mm × 1 mm (or 1 mm³). However, more recently, *high-resolution MRI*, also often called *magnetic resonance microscopy (MRM)*, has become feasible through the use of high-field magnets. Resolutions of 100 μm³ and below are now available at research centers around the world. Currently, specimen sizes are restricted to whatever can fit in the magnet bore, currently limiting high-resolution MRI to small animals. Example slices are shown in Figure 2.6 for both human and mouse.

While high-resolution MR imaging allows for near-microscopic anatomical assessment of small animals, the technology is not without tradeoffs (Mcconville et al., 2005). Improved resolution comes at the potential expense of scan time and loss of sensitivity. A significant increase in scan time may require that the animals be either heavily sedated in order to prevent motion, or scanned post-mortem altogether. On the other hand, decreased sensitivity results in a loss of dynamic contrast, which

along with spatial resolution, contribute to the detail of the scanned image. In addition, the high-field magnets may result in image instabilities, such as intensity and spatial inhomogeneities (Sled et al., 1998; Leow et al., 2006). As this paper is focused on post-acquisition image processing algorithms, the reader is referred to the book, *Principles of Magnetic Resonance Imaging* by Dwight Nishimura, for a more thorough examination of classical principles and methods (Nishimura, 1996).

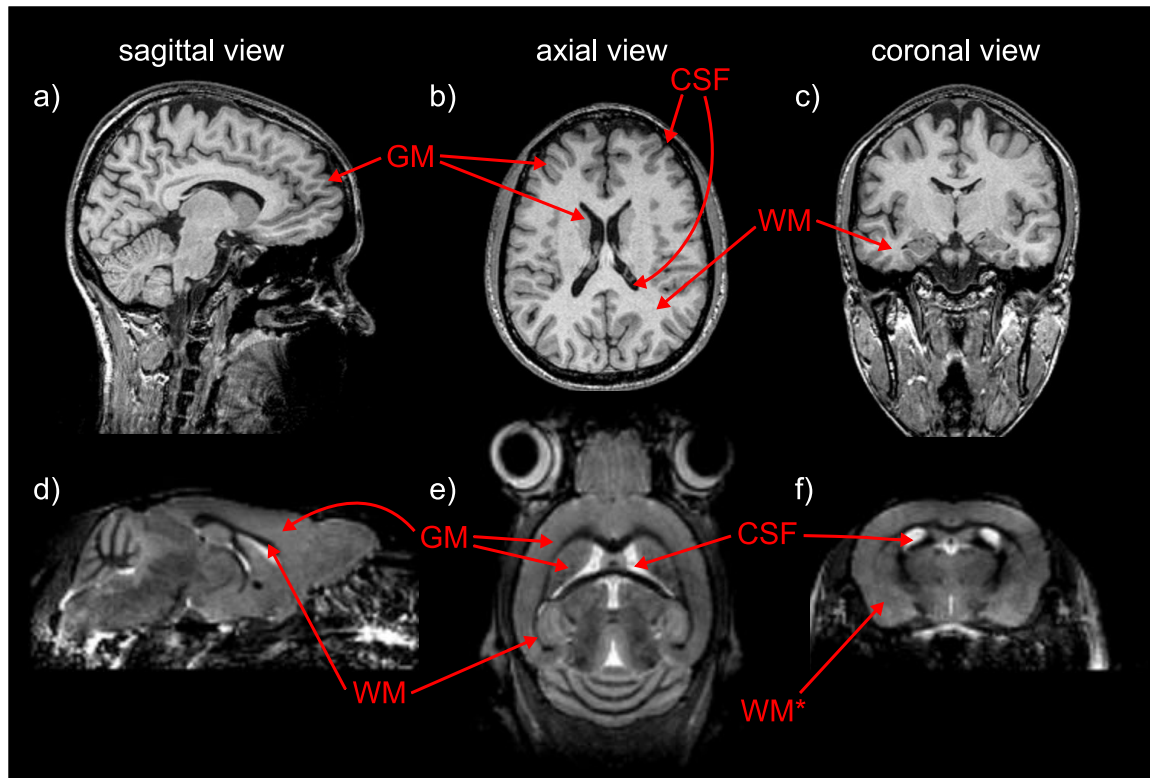


Figure 2.6: Example slices from a human T_1 -weighted image (a-c), and a mouse T_2 -weighted image (d-f) in the three standard viewing planes. In a T_1 -weighted image, GM appears gray, CSF appears dark, and WM appears white. In a T_2 -weighted image, GM appears gray, CSF appears white, and WM appears dark. Indicators are included for the various tissue types. WM* indicates a region where WM is expected but cannot be resolved at the acquired resolution. Note the obvious difference in cortical complexity of the human and mouse brains.

2.3 Manual Segmentation

Traditionally, human MRI studies have employed manual or semi-automated methods to examine cross-sectional and longitudinal structural effects. These *in vivo* studies have helped to reveal atrophy of the corpus callosum (Hempel et al., 1998; Teipel et al., 2002), and regions of the entorhinal cortex and hippocampus (Xu et al., 2000), as well as expansion of the lateral ventricles (Bradley et al., 2002) in AD subjects. Manual volumetry has also been used to examine structural alterations in transgenic AD and wild-type mice (Redwine et al., 2003; Delatour et al., 2006; Oberg et al., 2007). These volumetric studies appear to be consistent with findings in humans, revealing that whole brain and hippocampal volumes are significantly reduced in TG mice, while ventricular volume was enlarged, when compared to their wild-type (WT) littermates (Figure 2.7) (Delatour et al., 2006; Oberg et al., 2007).

While manual segmentation and visual inspection methods have yielded numerous important findings related to the characterization and diagnosis of AD, they are time-consuming, prone to intra- and inter-operator variability and bias, and require *a priori* hypotheses about affected neuroanatomical structures. As such, these methods are inappropriate for large-scale and exploratory imaging studies. MR image processing, or *computational neuroanatomy*, techniques have been developed to facilitate analysis by providing an automated, and ideally, unbiased framework (reviewed by Ashburner et al., 2003; Evans, 2005).

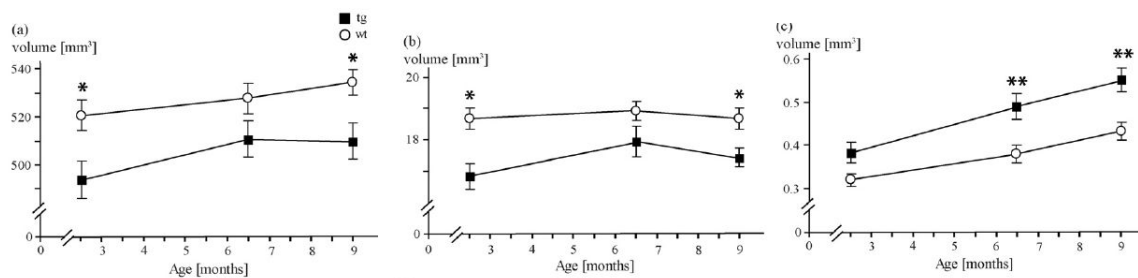


Figure 2.7: Manual volumes for (a) whole brain, (b) hippocampus, and (c) ventricles in TG and WT mice across three timepoints. Volume is reduced in whole brain and hippocampus measures in tg, and increased in the ventricular volume (Oberg et al., 2007) (tg = APP/PS1; wt = wild-type).

2.4 Computational neuroanatomy

In human MRI studies of AD, computational neuroanatomy approaches have helped to automate, or at least semi-automate, the detection of structural abnormalities in affected cortical, subcortical, ventricular, and hippocampal regions (reviewed by Grenander and Miller, 1998; Anderson et al., 2005; Evans, 2005; Barnes et al., 2007; Thompson et al., 2007). Whole brain morphometric studies have revealed a limbic-to-frontal structural progression of pathology (Fox et al., 2001; Janke et al., 2001; Thompson et al., 2003; Lerch et al., 2005, 2006) that is consistent with the underlying staging described by Braak on post-mortem brains (Braak and Braak, 1991). Furthermore, automated analyses of the hippocampus (Crum et al., 2001; Thompson et al., 2004) and ventricles (Ferrarini et al., 2006) have revealed focally affected regions within these structures in AD subjects.

Equivalent automated solutions for the study of mouse neuroanatomy have thus far remained largely unexplored. This thesis serves to investigate computational neuroanatomy methods for characterizing mouse models of AD in the context of a longitudinal MRI dataset of TG and WT mice. The following sections represent a synopsis of three general methodologies for automated analysis of brain morphology:

1. Atlas-based segmentation
2. Tissue classification
3. Deformation-based morphometry

2.4.1 Atlas-based segmentation methods

Brain atlases have provided a way of consolidating neuroimaging results across sites and laboratories. They consist of individual or group efforts to delineate neuroanatomical structures in a way that aims to facilitate standardized reporting of study results. Brain research in humans has shifted over the years from mappings of individual post-mortem neuroanatomy from histological slices (Talairach and Tournoux, 1988), to digital stereotaxic templates of normal populations (Mazziotta et al., 1995; Collins

et al., 1995; Mazziotta et al., 2001), normal individuals (Holmes et al., 1998), as well as age- or disease-specific brains (Evans, 2005; Thompson et al., 2007). Typically, using 3D warping or nonlinear registration algorithms (reviewed by Woods et al., 1998; Robbins et al., 2004), template-based anatomical labels can be propagated onto individual brain scans, eliminating the need to segment each MRI volume manually (Bajcsy and Kovacic, 1989; Collins et al., 1995; Crum et al., 2001; Castellanos et al., 2002; Hsu et al., 2002; Fischl et al., 2002; Walhovd et al., 2005; Heckemann et al., 2006). Anatomical labels of the brain atlas have traditionally been defined using discrete values, where a single neuroanatomical structure is defined at each brain voxel. However, more recently, brain MRI researchers have shifted toward segmentation of structures using probabilistic labels of neuroanatomical structures (Fischl et al., 2002). This method has the added advantage that it utilizes information about intersubject anatomical variability in assigning a label to each voxel of the subject MRI.

Atlas-based segmentation methods allow for the quantification of regional brain volume. These values can be statistically assessed across populations or parameters of interest depending on the research paradigm as in manual segmentation studies of the past. For example, in a longitudinal study, Walhovd et al. (Walhovd et al., 2005) studied the effects of normal aging across 16 automatically segmented neuroanatomical structures. Changes in brain volume were found to exhibit regional heterogeneity, meaning that different brain regions exhibited different trajectories with age.

Rigorously defined stereotaxic coordinate systems from 2D histological sections are also available to rodent brain researchers (see Paxinos and Franklin, 2001). With the increasing availability of small animal MRI scanners, high-resolution individual (Chan et al., 2007) and population MRI atlases (Dhenain et al., 2001; MacKenzie-Graham et al., 2004; Ma et al., 2005; Kovacevic et al., 2005; Ali et al., 2005; Badea et al., 2007) have also been proposed and subsequently used for morphometric analyses. While atlas-based segmentation methods are evidently a powerful means of studying rodent MRI scans, several drawbacks exist that impede their routine use. First, these atlases are not often made publicly available. In addition, the available reference templates are not often scanned in an imaging modality or using specimen preparation methods that are compatible across sites or even studies. For example, the atlas proposed by MacKenzie-Graham et al. (MacKenzie-Graham et al., 2004) scanned

adult, laboratory mice *ex vivo* using a T_1 -weighted sequence, while the transgenic and wild-type mice studied in this thesis (see Section 3.3) were scanned *in vivo* using a T_2 -weighted protocol. Finally, developing an accurate and compatible atlas, if none already exists, is a labour-intensive endeavour that includes all the aforementioned drawbacks associated with manual segmentation (see Section 2.3).

2.4.2 Tissue classification methods

Tissue classification, essentially a generalized form of anatomical segmentation, is another common approach for morphometric analysis used in brain MR studies. The technique involves segmentation of tissue types rather than different neuroanatomical regions. As described in Section 2.2, MRI can produce images with a wide range of tissue contrast. Using any of a variety of pattern classification strategies (an excellent reference is Duda et al., 2000), the acquired MR volume can be classified into GM, WM, and CSF on a voxel-by-voxel basis. The most robust and accurate tissue classification methods are guided by supervised learning on training voxels in the target image, which are derived from a template in which the tissue types are known (Zijdenbos et al., 1994; Reddick et al., 1997; Cocosco et al., 2003). Generally, the application of intensity nonuniformity correction prior to classification improves performance (Sled et al., 1998).

The resulting tissue-classified maps can be further examined using voxel-based morphometry (VBM) or cortical surface-based analysis. VBM detects changes in the voxelwise tissue distribution after linear registration of MRI scans, usually in the context of *gray matter density* (Ashburner and Friston, 2000). Controversy over the original method (Bookstein, 2001) has led to a refined version called *modulated* or *optimized* VBM that applies nonlinear warping prior to analysis (Good et al., 2002; Ashburner and Friston, 2001; Davatzikos et al., 2001). Cortical surface techniques require extracting the GM-pial and the WM-GM surface meshes from the voxelwise tissue maps, most frequently using deformable modeling algorithms (Dale et al., 1999; MacDonald et al., 2000; Thompson et al., 2004). Subsequent analysis using vertex-based cortical thickness measures has been shown to be a sensitive and robust method for detecting cortical alterations *in vivo* (Lerch and Evans, 2005).

There are, however, few studies that address the challenges associated with rodent tissue classification. Only one published study, by Schwarz et al. (Schwarz et al., 2006), has proposed tissue probability maps for rodent neuroimaging, but their framework was implemented only for rat MR images, utilized only two tissue classes (brain and CSF), and has not been made publicly available. One of the main difficulties with rodent tissue classification lies in the relatively reduced proportion of white matter relative to total brain tissue. WM represents only approximately 5–8% of total brain volume in mice (Ma et al., 2005) compared to 30–35% in adult humans (Good et al., 2001). In addition, due to current limitations in resolution for *in vivo* MRI, many voxels containing WM cannot be properly resolved due to partial volume effects. WM tracts of mice and rats constitute only a thin, and at times subvoxel, boundary between cortical GM and subcortical structures (Figure 2.6). Algorithms that correct for partial volume effects (Tohka et al., 2004) may improve classification. As well, one novel proposal by Tohka et al., employs genetic algorithms and an unsupervised learning strategy to classify images, which may be worthy of future investigation (Tohka et al., 2007).

2.4.3 Deformation-based morphometry

The lack of a standardized stereotaxic atlas for automated segmentation, as well as the unresolved issue of murine tissue classification, suggest that alternative computational neuroanatomy strategies need to be explored. One possibility, and the one that is investigated in this thesis, is *deformation-based morphometry* (DBM), also known as tensor-based morphometry or voxel-compression mapping. DBM is a well-established, automated method that can detect localized, morphological changes or differences using information contained in the vector field required to nonlinearly register MR images (Davatzikos et al., 1996; Bookstein, 1997; Thompson and Toga, 1997; Ashburner et al., 1998; Cao and Worsley, 1999; Chung et al., 2001; Janke et al., 2001). The approach is exploratory and provides local information about neuroanatomically affected regions. In addition, DBM is almost entirely *data-driven* meaning that, apart from the selection of a reference space to which all MR images are registered, it relies on only the original image volumes themselves. This method has also been applied prospectively for single subject analysis (reviewed by Ashburner et al., 2003), but we focus here on its application to the study of populations.

DBM has recently been applied to study MR images of normal (Kovacevic et al., 2005; Chen et al., 2006; Spring et al., 2007) and transgenic mice (Nieman et al., 2006). For this purpose, registration strategies that have been validated and employed in numerous human neuroimaging studies (Collins et al., 1995; Woods et al., 1998) have been adapted for use on rodent images (Kovacevic et al., 2005; Chen et al., 2006). In fact, murine brains are particularly well-suited for this form of analysis due to their relatively homogeneous morphology (recall Figure 2.6). On the other hand, in humans, the variability in cortical folding has presented some practical issues for proper, nonlinear registration and subsequent DBM analysis (Ono et al., 1990; Woods, 1996).

An unbiased, population-specific reference space

One of the most important implementation decisions in a DBM analysis is the selection of an appropriate reference space (or template) for spatial normalization. Typically, input MR images are warped to an individual representative image from the population (Studholme et al., 2004), or a publicly available stereotaxic template (e.g. Mazziotta et al., 2001). Of course, the best template would be one that is able to finely match structures across all MR images included in a given study. Several strategies for template generation have been proposed and subsequently evaluated in the literature (Kochunov et al., 2001; Rohlfing et al., 2004; Kovacevic et al., 2005; Christensen et al., 2006). Kochunov et al. developed a means of quantitatively selecting a *minimum deformation target*, or best individual template, from the original MR scans (Kochunov et al., 2001).

More recently, Kovacevic et al. developed an unbiased reference creation algorithm, or *minimum deformation average* approach, for mouse MR images (Kovacevic et al., 2005). Their technique, summarized in Figure 2.8 and Section 3.3.2, is unbiased in the sense that it does not rely on nonlinear registration to a prior template, but instead produces a nonlinear reference space from the input population itself. This data-driven technique is mediated by a pairwise registration algorithm that registers each input scan to every other input scan in the dataset, and averaging the resulting transformations. The deformation fields required to nonlinearly register individual scans to this population average are then evaluated as part of a deformation-based

analysis.

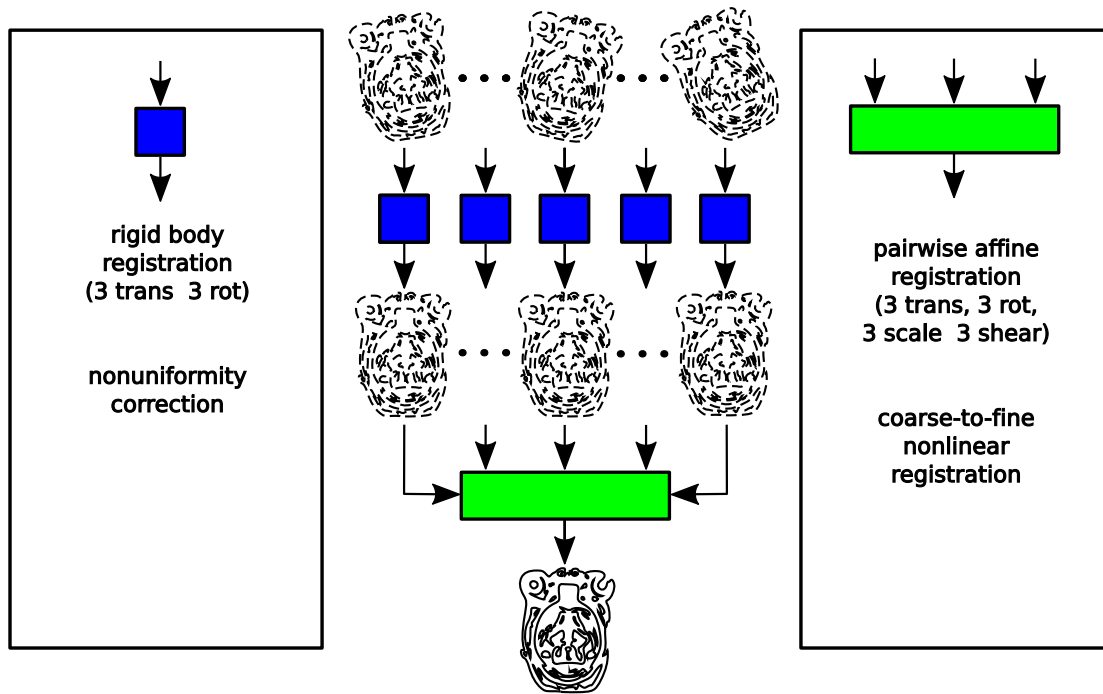


Figure 2.8: Illustration of the unbiased reference creation image processing pipeline described by Kovacevic et al. (Kovacevic et al., 2002). The pipeline uses tools developed at the Brain Imaging Centre that have been made freely available to the neuroimaging community.

Computing the Jacobian determinant

In population-based MRI studies, DBM typically quantifies the local voxelwise growth or atrophy in the brain based on the nonlinear registration of MRI scans to a reference space. The nonlinear transformation is manipulated in order to obtain a unified voxelwise mapping, $\mathbf{T} = (T_1, T_2, T_3)$ defined at every voxel $\mathbf{x} = (x_1, x_2, x_3) \in \mathbb{R}^3$, from reference space to the native space of each scan. The Jacobian matrix, or Jacobian *tensor*, at every voxel can then be expressed as:

$$\mathbf{J}(\mathbf{x}) = \frac{\partial \mathbf{T}(\mathbf{x})}{\partial \mathbf{x}} = \begin{bmatrix} \frac{\partial T_1(\mathbf{x})}{\partial x_1} & \frac{\partial T_1(\mathbf{x})}{\partial x_2} & \frac{\partial T_1(\mathbf{x})}{\partial x_3} \\ \frac{\partial T_2(\mathbf{x})}{\partial x_1} & \frac{\partial T_2(\mathbf{x})}{\partial x_2} & \frac{\partial T_2(\mathbf{x})}{\partial x_3} \\ \frac{\partial T_3(\mathbf{x})}{\partial x_1} & \frac{\partial T_3(\mathbf{x})}{\partial x_2} & \frac{\partial T_3(\mathbf{x})}{\partial x_3} \end{bmatrix} \quad (2.1)$$

From this 3x3 matrix, the Jacobian determinant, or simply the *Jacobian*, is most often computed as a summary measure of local volume:

$$J(\mathbf{x}) = \left| \frac{\partial \mathbf{T}(\mathbf{x})}{\partial \mathbf{x}} \right| \quad (2.2)$$

This metric has been shown to provide a simple and direct means of determining local, voxelwise morphometric changes (growth or atrophy) relative to the reference space. Once the Jacobian maps have been computed for the dataset, local patterns of brain change and structural differences can be evaluated using an appropriate statistical framework.

2.5 Longitudinal analysis

Until fairly recently, most neuroimaging studies have been cross-sectional in nature, requiring relatively simple statistical tests for the assessment of group differences. As large-scale MRI studies with longitudinal designs are becoming increasingly common (Castellanos et al., 2002; Mueller et al., 2005; Evans, 2006), the neuroimaging community has begun to embrace mixed-effects models for the analysis of neurostructural changes (e.g. Resnick et al., 2003; Shaw et al., 2006; Walhovd et al., 2005). Mixed-effects regression provides a framework for examining longitudinal grouped data. Mixed-effects regression is so named because it involves a combination of *fixed* and *random* effects for the modelling of parameters/observations as related to a given outcome measure. Fixed effects are modelled on entire populations or groups within the dataset, while random effects are associated with individual units within the study population. This flexible statistical framework allows for the handling of both balanced and unbalanced data, repeated measures, and modelling of any number of effects and interactions. The text by José Pinheiro and Douglas Bates, entitled *Mixed-Effects Models in S and S-Plus*, provides an excellent introduction into this realm of statistics and computing.

The application of DBM to longitudinal data with more than two timepoints is a relatively novel prospect. Longitudinal AD-related DBM studies have, to this

point, been limited, even in human MRI studies (Janke et al., 2001). While Verma et al. have utilized DBM in their studies of murine development (Verma et al., 2005; Zhang et al., 2005), their method has relied on semi-automated, tag point-guided registration. Their statistical analyses were also limited to a set of manually segmented regions-of-interest, rather than a unified voxelwise assessment across a reference MRI volume.

2.6 Research justification

To date, there have been no MRI studies that have examined longitudinal morphological effects in mouse models of AD using computational neuroanatomy approaches. This thesis investigates the viability of an unbiased reference creation algorithm, in conjunction with deformation-based morphometry, to characterize morphological age-related patterns in double transgenic APP/PS1 mice and their wild-type littermates in an exploratory fashion. A statistical framework based on mixed-effects regression was also designed and evaluated.

Preface to Chapter 3

The experiments and results of the thesis are presented in manuscript-based form. The following paper, accepted and published in *NeuroImage*, investigates the application of DBM to the longitudinal study of a transgenic model of AD. In accordance with the McGill University Thesis Preparation and Submission Guidelines (Section I.C.), the paper has been included in its entirety. Other works related to the current Master's project, but not included in the thesis, are listed for reference.

Contributions from Current Research Included in the Thesis

1. Jonathan C. Lau, Jason P. Lerch, John G. Sled, R. Mark Henkelman, Alan C. Evans, Barry J. Bedell. Longitudinal Neuroanatomical Changes Determined by Deformation-Based Morphometry in a Mouse Model of Alzheimer's Disease. *NeuroImage*. 2008. Accepted.

Contributions from Current Research Not Included in the Thesis

1. Barry J. Bedell, Alex P. Zijdenbos, M. Mallar Chakravarty, Jonathan C. Lau, D. Louis Collins, Alan C. Evans. An Integrated Technology Platform for the Study of Animal Models of CNS Disease. *The 12th Annual Meeting of the Organization for Human Brain Mapping*. Florence, Italy. June 11-15, 2006.
2. Jonathan C. Lau, Jason P. Lerch, Tomas Klason, Barry J. Bedell, Alan C. Evans. A Longitudinal MRI Study of Disease Progression in APP/PS1 Mice Using Deformation-Based Morphometry. Hot Topics Poster. *The 10th International Conference on Alzheimer's Disease and Related Disorders*. Madrid, Spain. July 15-20, 2006.

3. Jonathan C. Lau, Jason P. Lerch, John G. Sled, R. Mark Henkelman, Alan C. Evans, Barry J. Bedell. Comparing Automatic Deformation-Based Techniques Against Manual Volumetry in a Mouse Model of Alzheimer's Disease: A Longitudinal *In Vivo* Study. Electronic poster. *Joint Annual Meeting of the 15th International Society for Magnetic Resonance in Medicine and the 27th European Society for Magnetic Resonance in Medicine and Biology*. Berlin, Germany. May 19-25, 2007.
4. Jonathan C. Lau, Jason P. Lerch, Simone P. Zehntner, Edith Hamel, Alan C. Evans, Barry J. Bedell. Poster. Identifying the Trajectory of Disease in APP/PS1 Mice using Automated Deformation-Based Analysis with Manual Validation. *The 2nd International Conference on Prevention of Dementia*. Washington, D. C., United States of America. June 9-12, 2007.

Chapter 3

Manuscript for *NeuroImage*

**Longitudinal Neuroanatomical Changes
Determined by Deformation-Based Morphometry
in a Mouse Model of Alzheimer's Disease**

Jonathan C. Lau^a, Jason P. Lerch^b, John G. Sled^b,
R. Mark Henkelman^b, Alan C. Evans^a, and Barry J. Bedell^a

NeuroImage. 2008. Accepted.

^a McConnell Brain Imaging Centre, Montreal Neurological Institute,
McGill University, 3801 University Street, Montreal, QC, Canada H3A 2B4

^b Mouse Imaging Centre, Hospital for Sick Children,
555 University Avenue, Toronto, Ontario, Canada M5G 1X8

3.1 Abstract

Magnetic resonance imaging (MRI) of transgenic mice has the potential to provide valuable insight into the complex mechanisms underlying Alzheimer’s disease (AD). Quantification of pathological changes is typically performed using manual segmentation methods, and requires *a priori* hypotheses about anatomical structures for volumetric measurement. Alternatively, deformation-based morphometry (DBM) has been shown to be a powerful, automated technique for detecting anatomical differences between populations by examining the deformation field used to nonlinearly warp MR images. In this multiple timepoint *in vivo* study, we have applied an automated, unbiased technique for the creation of a nonlinear, population-specific reference space from which robust DBM analysis can be performed. A general, linear mixed-effects model framework was developed to follow the evolution of structural changes in mouse brain from 2.5 to 9 months of age, and to examine neuroanatomical differences between a transgenic (TG) APP/PS1 murine model of AD and wild-type (WT) littermates. Morphometric abnormalities in the TG group were localized to regions of the hippocampus, cortex, olfactory bulbs, stria terminalis, brain stem, cerebellum, and ventricles. Although volumetric reductions were detected in TG mice, no general brain atrophy was found, suggesting a developmental, rather than a degenerative, pathological process. Finally, we established a strong correlation between a DBM summary measure and manually segmented volumes for each image in the dataset. These results support the utility of DBM to study longitudinal morphological changes in mouse models of central nervous system diseases in an automated and exploratory fashion.

3.2 Introduction

Alzheimer’s disease (AD) is a devastating neurodegenerative disease that currently afflicts over 4.5 million people in the U.S., and which is predicted to rise to 11.3–16 million by 2050 (Hebert et al., 2003). This staggering prevalence and rapidly growing incidence point to the desperate need for the development of new therapeutic avenues for the treatment of AD. While currently available drugs provide limited, short-term, symptomatic effects, drug development has moved toward disease-modifying therapies

which would slow, reverse, or ultimately prevent AD. These disease-modifying agents are, generally, designed for molecular targets known to be involved in the pathogenesis of AD. However, the ultimate phenotypic consequences of the expression of these molecular targets remain poorly understood.

Longitudinal, anatomical magnetic resonance imaging (MRI) studies provide a non-invasive means of following the subtle structural changes which occur during the natural evolution of AD (Lerch et al., 2005). While most quantitative MRI studies of AD-related neuroanatomical alterations have focused on human subjects (see reviews by Anderson et al., 2005; Barnes et al., 2007; Thompson et al., 2007), a few recent studies have examined volumetric changes in transgenic (TG) mouse models of AD (Redwine et al., 2003; Delatour et al., 2006; Oberg et al., 2007). TG murine models with targeted expression of mutated amyloid precursor protein (APP) genes demonstrate many of the cognitive (Palop et al., 2003) and neuropathological features of AD, including senile plaques, neuronal impairments, acetylcholine (ACh) denervation (Hsia et al., 1999; Mucke et al., 2000; Aucoin et al., 2005), cerebral hypometabolism (Niwa et al., 2002), and alterations in synaptic transmission (Larson et al., 1999). These models are particularly useful for studying the natural evolution of AD, as well as for evaluation of the therapeutic efficacy of new disease-modifying agents.

Quantitative anatomical MRI studies of TG models of AD have largely been limited to manual segmentation of regions-of-interest (ROIs) (Redwine et al., 2003; Delatour et al., 2006; Oberg et al., 2007). These techniques, however, are labour-intensive, prone to intra- and inter-rater bias, relatively insensitive to subtle morphological brain changes (Ashburner et al., 2003), and require *a priori* hypotheses about affected anatomical structures, thereby excluding potentially relevant regions from the analysis.

In order to overcome these inherent limitations, we have developed an alternative automated approach, using deformation-based morphometry (DBM), to detect the natural evolution of neuroanatomical changes in TG mouse models of AD. DBM is a quantitative image analysis technique which evaluates information contained within the vector field generated by the nonlinear warping of an individual MRI scan to a reference template (Davatzikos et al., 1996; Bookstein, 1997; Thompson and Toga, 1997; Ashburner et al., 1998; Cao and Worsley, 1999; Chung et al., 2001). In contrast

to voxel-based morphometry (VBM) (see Ashburner and Friston, 2000; Good et al., 2001; Bookstein, 2001; Ashburner and Friston, 2001), DBM does not require segmentation of the brain into different tissue compartments, which can be particularly challenging in the murine brain. Further, DBM has been successfully applied to examine cross-sectional morphological differences and longitudinal anatomical changes in human (Fox et al., 2001; Janke et al., 2001; Studholme et al., 2004; Leow et al., 2006) and, more recently, mouse neuroimaging studies (Verma et al., 2005; Zhang et al., 2005; Chen et al., 2006; Nieman et al., 2006; Spring et al., 2007). While the majority of DBM studies of mouse brains have been limited to cross-sectional or dual timepoint studies, Verma et al. (Verma et al., 2005) and Zhang et al. (Zhang et al., 2005) recently extended this technique to study murine brain development over multiple timepoints, comparing changes in diffusion-tensor MR images of fixed *ex vivo* brains between post-natal developmental stages using qualitative, landmark-, and ROI-based quantitative measures.

In the present study, we have utilized DBM to examine *in vivo* neuroanatomical differences between TG mouse models of AD and wild-type (WT) littermates, as well as followed the evolution of these structural changes from 2.5 to 9 months of age using a general, linear-model framework based on the deformation maps. The relationship between the results of our automated analysis and conventional manual segmentation methods was assessed for a number of different anatomical structures. This fully-automated framework allows for voxelwise statistical analysis and obviates the need to specify pre-determined ROIs, thereby resulting in an unbiased, exploratory method for analyzing subtle differences between TG and WT populations.

3.3 Materials and methods

3.3.1 Animals and MRI measurements

MRI scans were kindly provided by AstraZeneca R&D (AstraZeneca, Södertälje, Sweden). The mouse models and MRI scanning protocols used for these studies have previously been described, in detail, by Oberg et al. (Oberg et al., 2007). Briefly, 20 TG APP/PS1 mice (11 females, 9 males) and 13 WT littermates (11 females, 2 males)

were scanned at 2.5 months (14 TG, 9 WT), 4.5 months (13 WT, 9 WT), 6.5 months (10 TG, 10 WT), and 9 months (8 TG, 13 WT) of age for a total of 86 scans. MRI scans were performed using a horizontal-bore 9.4 T magnet (Bruker Biospec 94/30, Bruker, Ettlingen, Germany) equipped with a 12 cm inner-diameter self-shielded gradient system (maximum gradient strength 400 mTm^{-1}). A 72-mm volume coil was used for excitation and a quadrature mouse brain surface coil (Bruker, Germany) was used for signal detection. MR images were acquired with a 3D inversion-recovery, spin-echo sequence, with the following scan parameters: matrix size = $128 \times 128 \times 64$, FOV = $2.0 \text{ cm} \times 2.0 \text{ cm} \times 1.0 \text{ cm}$, resolution = $156.25 \mu\text{m} \times 156.25 \mu\text{m} \times 156.25 \mu\text{m}$, TR = 2500 ms, TE = 5.7 ms, RARE factor = 4, inversion delay = 500 ms, and NEX = 1. The total acquisition time was 1 h and 26 min.

3.3.2 Longitudinal deformation-based morphometry

Reference model and nonlinear registration

Image processing was performed using software available from the McConnell Brain Imaging Centre (<http://www.bic.mni.mcgill.ca/software>) at the Montreal Neurological Institute (Montreal, Canada). A single, average MRI reference space was generated using all 86 scans following the methods of Kovacevic et al. (Kovacevic et al., 2005). A representative scan was chosen as the prior model for initializing the reference model creation algorithm. The brain region of the representative scan was manually outlined using the Display software package (Montreal Neurological Institute, Montreal, Canada) yielding a brain mask for our initial model space. This brain mask was used for all subsequent reference model creation steps. Briefly, each scan was first registered using a rigid body (lsq6) transformation to the prior model (Collins et al., 1994). Next, images were corrected for intensity nonuniformity artifacts using the N3 algorithm (Sled et al., 1998) with nonuniformity correction limited to the brain-masked region of the model. The specific parameters utilized were: distance = 8 mm, FWHM = 0.15 mm, number of iterations = 100, and number of runs = 8. Pairwise 12-parameter (lsq12) registrations were then performed to create an unbiased affine average model of the entire dataset. This transformation was followed by a series of nonlinear registration steps, applied in a coarse-to-fine fashion, with each subsequent step using the best previous model as a registration target (Collins et al.,

1995; Kovacevic et al., 2005). After concatenating the sequential transformations, the scans were resampled and averaged, resulting in a population-specific model. The registration parameters are provided in Table 3.1.

The resulting deformation field, consisting of 200 μm grid points, was inverted. The linear terms were removed and the deformation field was centered to the average displacement across the entire population studied, allowing for the vector fields to be interpreted in a reference space. After resampling, the final deformation field provided a nonlinear mapping, $\mathbf{T}(\mathbf{x})$, from reference space to the native space of each scan at every voxel, \mathbf{x} .

Assessment of registration performance

Inaccuracies in reference model creation can occur due to warping to a finite voxel size (quantization) and imperfect/suboptimal calculation of the nonlinear transformation. In order to assess the registration performance of the reference model creation process, we utilized manual segmentation data for three neuroanatomical structures (whole brain, hippocampus, and lateral ventricles) that had been segmented in the native space of all 86 scans used in the study. The manual segmentations of these three structures were provided by AstraZeneca R&D (AstraZeneca, Södertälje, Sweden). The segmentation methods have been described, in detail, by Lavebratt et al. (Lavebratt et al., 2006) and Oberg et al. (Oberg et al., 2007). The manual segmentations of each MRI scan were run through an iterative loop as follows:

1. identify forward transformation between native space and reference space;
2. apply transformation to native structure segmentation to obtain a resampled segmentation in reference space.

A voxel overlap index was then calculated across all scans for each manually segmented structure. In principle, the reference space segmentations obtained from each scan should be identical. However, the aforementioned practical factors, as well as potential rater variation in the manual segmentation, may cause a mismatch at the structure border especially for low-dimensional transformations. The voxel overlap index was therefore assessed at progressively decreasing spatial resolution as follows:

1. every voxel in reference space was assigned a value between 0 and 100% (perfect overlap) for a given structure, corresponding to the proportion of the 86 scans for which that voxel included that structure;
2. maximal perfect overlap was defined as the peak number of voxels exhibiting perfect overlap across all registration stages;
3. a voxel overlap metric was computed according to the method utilized by Spring et al. (Spring et al., 2007), specifically:

$$\text{voxel overlap} = \frac{\text{voxels at stage with perfect overlap}}{\text{voxels at stage with maximal perfect overlap}} \quad (3.1)$$

Adaptive spatial filtering

In order to reduce noise in the deformation maps, we have applied the intensity consistent approach described by Studholme et al. (Studholme et al., 2003). This anisotropic filter was selected over more traditional Gaussian smoothing methods since it is edge-preserving and thus, better respects anatomical boundaries. Briefly, this algorithm performs a Gaussian blur, $f(\mathbf{k})$, at each voxel, \mathbf{x} , of the associated deformation field, where the contribution of each kernel neighbor, $\mathbf{k} \in K$, depends on the MR intensity-based statistical relationship, $p_{xk}(\mathbf{x}, \mathbf{x} - \mathbf{k})$, between \mathbf{x} and its relative neighbor $\mathbf{x} - \mathbf{k}$. The value of $p_{xk}(\mathbf{x}, \mathbf{x} - \mathbf{k})$ was computed from an estimate of the average and individual subject scan intensity within the local neighborhood, K (Studholme et al., 2003). The filtering equation can be formalized as

$$\tilde{\mathbf{T}}(\mathbf{x}) = \frac{1}{\Theta(\mathbf{x})} \int_{\mathbf{k} \in K} \mathbf{T}(\mathbf{x} - \mathbf{k}) \cdot f(\mathbf{k}) \cdot p_{xk}(\mathbf{x}, \mathbf{x} - \mathbf{k}) \cdot d\mathbf{k} \quad (3.2)$$

In order to account for the variable contribution of neighbors at each voxel,

$$\Theta(\mathbf{x}) = \int_{\mathbf{k} \in K} f(\mathbf{k}) \cdot p_{xk}(\mathbf{x}, \mathbf{x} - \mathbf{k}) \cdot d\mathbf{k} \quad (3.3)$$

was computed and used to normalize the local volume. A kernel width of 1.0 mm was used for filtering.

Computation of the Jacobian determinant

In order to examine the local volume change in each subject, the Jacobian determinant (or simply the Jacobian), $\tilde{J}(\mathbf{x})$, for each vector, $\tilde{\mathbf{T}}(\mathbf{x})$, in the filtered deformation field was computed at every voxel (Chung et al., 2001; Janke et al., 2001). This metric has been shown to provide a simple and direct means of determining local, voxelwise expansion or compression relative to the reference space. Global effects of size were reintroduced at every voxel by multiplying the local Jacobian by the scale term associated with the spatial linear normalization of each image to the reference space. The scaled Jacobian was log-transformed in order to better approximate a symmetric normal distribution, thereby permitting the use of a mixed-effects model.

3.3.3 Longitudinal statistical analysis of the voxelwise Jacobian

In order to characterize the local trajectory of change, mixed-effects models were tested at every voxel within the brain from the filtered, Jacobian maps. Mixed-effect models extend standard linear models by adding an additional error term that corresponds to the variable intercept for each subject in a longitudinal dataset with no requirement of balance in the data (i.e. it is not necessary for all mice to have the same number of scans) (Pinheiro and Bates, 2002). The nature of the Jacobian's relationship with age was modeled as a sum of fixed and linear components, and different polynomial models were evaluated for the developmental trajectory. Interactions with genotype and sex were assessed, and to account for within-subject dependencies, random effects for both intercept and slope for each individual were tested. For this analysis, age was centered to the mean age of the population. Finally, mixed-effects models were compared using voxelwise likelihood ratio tests, and the simpler model was chosen whenever it was found to explain most of the variance.

The resulting statistical maps were corrected for multiple comparisons using the

false discovery rate (FDR) procedure with $q = 0.05$ (Genovese et al., 2002). A single FDR threshold was determined by pooling the uncorrected P -values across all effects and all voxels tested. By taking into account the degrees of freedom for a given statistical test, a t -value threshold for each statistical map was computed from the FDR-determined P -value. Regions of significant group-dependent deformation were reported with the aid of a mouse atlas (Paxinos and Franklin, 2001). All statistical analyses were performed using the R software package (www.r-project.org) in conjunction with the nlme and RMINC libraries.

3.3.4 Relationship between DBM results and conventional manual volumetry

In order to examine the relationship between the automated results from DBM and manual volumetric analyses, we studied the longitudinal patterns of change in manual segmentations of whole brain, hippocampus, and lateral ventricles using mixed-model regression. We evaluated registration performance across all 86 subjects studied. These segmentations were used to assess the same mixed-effects components as in the longitudinal statistical analysis for DBM.

We examined the relationship between an automated measure of volume computed from the nonlinear transformations and the manually segmented volumes for all 86 scans. The volume of interest for each structure was derived from the probabilistic average of all individual manual segmentations, thresholding the 3D probability map at 50% and manually correcting the borders. Subsequently, these reference masks for each structure were transformed back into the native space of each scan using the previously computed nonlinear transformations, thereby providing an automated estimate of the actual volume. The correlation between the automated volume and the manually segmented volume for each scan and structure was then determined.

3.4 Results

3.4.1 Reference model and nonlinear registration

Prior to the DBM analysis, the quality of registration was assessed in order to ensure that reference creation had been properly performed. Figure 3.1a depicts the qualitative improvements that can be observed over the course of reference model creation. The variability of neuroanatomical features decreased with pipeline progression, particularly in white matter structures (e.g. the cerebellar and dorsal hippocampal commissures), and the ventricles. The extra-axial tissues remained highly variable since they were excluded from the registration steps. Figure 3.1b shows the quantitative improvement using our voxel overlap metric. Improvements were observed to plateau following six generations of nonlinear registration.

3.4.2 Results of longitudinal DBM analysis

The voxelwise, log-transformed Jacobian provides a biologically interpretable measure of local volumetric expansion (> 0) or compression (< 0) relative to the reference space. Mixed-effects models were tested and compared across all voxels in the brain using ANOVA. We tested main effects of gender, as well as interactions of gender with age and genotype. However, the inclusion of these terms did not result in any significant effects in the analysis. As such, the final statistical model included fixed-effects for genotype (β_1), age (β_2), and the interaction of genotype with age (β_3), as well as a random intercept to account for within-subject variability (b_i). This simple model was found to be as robust as more complicated models (e.g. modeling both slope and intercept as random effects). Thus, for each subject i , the model evaluated was

$$J_i(\mathbf{x}) = \beta_0 + b_i + \beta_1 \times \text{genotype} + \beta_2 \times \text{age} + \beta_3 \times \text{age} \times \text{genotype} + \epsilon \quad (3.4)$$

where β_0 represents the intercept term and ϵ is the residual error in the model. The

results from the analysis showed significant patterns of local shape change that can be described on the basis of these underlying model components. Each component provides different information about local shape change. A significant age term is an indicator of local volume growth or loss with genotype effects removed. A significant genotype term indicates regions demonstrating inherent genetic differences between groups, in particular, where WT is larger than TG (reduction) and where TG is larger than WT (expansion) with age effects removed. Finally, a significant interaction between genotype and age signifies a region affected differently by aging in each groups. This interaction component is dependent on the values of both the age and genotype terms, and thus the direction of change was interpreted on a region-by-region basis.

Significant growth for both groups of animals was detected throughout the brain particularly in the hippocampus, olfactory bulbs, thalamus, cerebellar commissure, ventricles, and white matter tracts (e.g. anterior commissure and corpus callosum). Significant volume reduction was noted in several cortical regions (entorhinal, piriform, somatosensory), as well as in the caudate.

Neuroanatomical regions displaying significant genetic differences in volume are summarized in Table 3.2 for simple differences related to genotype and Table 3.3 for more complex, dynamic interactions between age and genotype. No interactions with sex were observed in the population studied. Representative regions of significant morphological change or difference are shown in Figure 3.2. The dynamics of longitudinal change are illustrated using voxelwise regression plots at specific, significant individual voxels of the hippocampus and other brain structures (entorhinal cortex, lateral ventricles, bed nucleus of the stria terminalis) in Figures 3.3 and 3.4, respectively.

3.4.3 Longitudinal findings from manual segmentations

While Figures 3.3 and 3.4 demonstrate the results of the automated voxel-based analysis, we also assessed the temporal dynamics for larger structures using the manual segmentation data. The best-fit, mixed-effects regression plots for each of the manually segmented structures, specifically whole brain, hippocampus and lateral

ventricles, are shown in Figure 3.5. All three structures exhibited significant linear growth ($P < 0.0001$).

Differences due to genotype (TG versus WT) were found in all three manually segmented structures. In TG mice, whole brain and hippocampus demonstrated reduced volume, while the lateral ventricles showed enlarged volume relative to WT. Significant interactions between age and genotype components in the hippocampus and lateral ventricles, and marginal interactions in the whole brain measure ($P = 0.054$) suggested an additional dynamic difference between groups that varied with age.

3.4.4 Correlation between automated and manually segmented measures

The correlation plots between the automated and manually segmented volumes for whole brain ($r = 0.97$; $P < 0.0001$), hippocampus ($r = 0.86$; $P < 0.0001$) and lateral ventricles ($r = 0.72$; $P < 0.0001$) are shown in Figure 3.6. While still highly significant, the lateral ventricles demonstrated the greatest variability in the correlation plot (Figure 3.6c).

3.5 Discussion

In this work, we have examined morphological changes and differences in a longitudinal, anatomical MRI study of TG APP/PS1 mice and WT littermates using DBM. The analysis was performed using a unified, population-specific reference space and mixed-effects modeling to allow for a voxelwise study of the distribution of age-related volumetric changes and regional differences related to genotype (i.e. TG vs. WT).

We found strong, positive correlations between results computed using our automated methods and manual segmentation/volumetry in selected anatomical structures for all 86 scans (see Figure 3.6). However, small offsets are evident in Figure 3.6b and 3.6c, indicating a systematic bias inherent in the automated method. Not

surprisingly, this bias becomes more evident as the size of the segmented structure decreases, with the greatest deviations observed in the lateral ventricles (see numerical scales on the axes of the plots in Figure 3.6). Nevertheless, the highly significant correlation analysis ($P < 0.0001$) justifies the use of reproducible, automated segmentation rather than manual approaches that suffer from intra-/inter-rater variability.

While a range of different longitudinal patterns were observed throughout the brain, emphasizing the heterogeneous nature of neuroanatomical changes, a number of distinct patterns identified in this study were particularly interesting. Growth with age was identified in the hippocampus, olfactory bulbs, thalamus, ventricles, cerebellar commissure, and white matter tracts in both TG and WT groups. On the other hand, age-related volume loss was identified in the lateral entorhinal, piriform, and somatosensory cortices, as well as the caudate nucleus.

A number of expected and unexpected findings were discovered upon examining genotypic differences. Volume reduction was observed in the cingulate, retrosplenial, and primary somatosensory cortices of TG mice relative to their WT littermates. Substantial β -amyloid pathology has been shown in these regions in both TG AD mouse models (Trinchese et al., 2004; Delatour et al., 2006; Oberg et al., 2007) and human AD patients (Braak and Braak, 1991). Reduced volumes were also noted in the olfactory bulb and piriform cortex of TG mice. This finding is supported by previous observations of olfactory dysfunction in AD patients (Thompson et al., 1998; Attems et al., 2005), and in the Tg2576 APP mouse model of AD (Smith et al., 2007). Several white matter tracts, particularly the anterior commissure, corpus callosum, internal capsule, and dorsal hippocampal commissure, also showed localized reductions in size in TG mice relative to their WT counterparts. Developmental abnormalities in the fiber connections may help to interpret the anatomical underpinnings of cognitive impairment in the studied TG model (Howlett et al., 2004; Trinchese et al., 2004). Volume reduction was also observed in the cerebellar paraflocculus and regions of the cerebellar commissure in the TG group. While the cerebellum generally remains unaffected in AD patients, the development of AD pathology in the cerebellum has been reported in early-onset patients with PS1 mutations (Larner and Doran, 2006).

Several neuroanatomical regions demonstrated volume expansion in TG mice such as the lateral and third ventricles. Enlargement of these particular regions has been observed in volumetric studies of this transgenic murine model (Delatour et al., 2006;

Oberg et al., 2007). In brain parenchyma, the bed nuclei of the stria terminalis, as well as the dorsal superior colliculus and periaqueductal gray of the brain stem, also demonstrated relative enlargement in the TG group. Interestingly, hypertrophy of the bed nuclei has been observed in studies of late-stage AD patients due to enlargement of galanin-containing fibres within the cholinergic basal forebrain (Mufson et al., 1993), while extensive plaque deposition in the brain stem has also been previously reported (Iseki et al., 1989).

By examining the interaction term between genotype and age, we were able to elucidate regions with difference in aging between TG and WT groups. As previously mentioned, these dynamic effects are dependent on both the local value of the age and genotype terms and, therefore, must be interpreted on a region-by-region basis. For example, a significant positive effect was observed in a focal portion of the left entorhinal cortex in WT versus TG. Detailed examination revealed relative volume growth with age in WT mice, while no change was detected in the same region of TG animals (Figure 3.4a). Regions within the retrosplenial granular cortex, ventrolateral hippocampus, and flocculus demonstrated age-related growth in WT mice, while observed suggested volumetric decline, or atrophy, in TG mice. With the exception of the flocculus, these regions are all known to be affected in the progression of disease in human (Braak and Braak, 1991; Lerch et al., 2005) and mouse models of AD (Hsia et al., 1999; Reilly et al., 2003; Palop et al., 2005).

The primary somatosensory, retrosplenial, cingulate, and piriform cortical regions exhibited smaller baseline volumes in the TG mice compare to WT mice, but are shown to increase in volume over the age range studied. This finding suggests that a process of delayed development had occurred and concurs with the hypothesis proposed by Delatour et al. (Delatour et al., 2006) describing a process of interrupted normal growth in TG mice in certain brain regions. Given that the mutant APP transgene is constitutively expressed, it is not surprising that phenotypic differences are evident at a young age.

Interestingly, there was a lack of general atrophy in TG mice relative to their WT littermates aside from a few, very focal regions within the dorsolateral hippocampus, retrosplenial cortex, and cerebellum. Instead, most of the anatomical differences appeared to result from a developmental, rather than a degenerative, process. These results, of course, require rigorous correlation with microscopic/molecular studies to

better understand the neuropathological changes underlying these gross morphological changes.

In this study, mixed-effects analysis was limited to applying a single statistical model across all brain voxels. Based on the plots of individual trajectories in Figures 3.3 and 3.4, it is apparent that a linear model may not be optimal for all cases. However, given the relatively small sample size of this study, we have been cautious in model selection in order to avoid over-interpreting the data using insufficiently powered higher-order models. Future studies with larger sample sizes and the inclusion of later timepoints may employ modeling with higher-order curvilinear components. For example, a step-down model selection algorithm, where each voxel would be fit with the polynomial mixed-effects model that best explains the variance, may allow for more detailed characterization of developmental trajectories (e.g. Shaw et al., 2007). We originally tested for main effects of gender, as well as interactions of gender with age and genotype. However, the inclusion of these terms did not result in any significant effects in the analysis. These terms were, therefore, removed in favour of a simpler model omitting gender as a covariate (see Equation 3.4). While gender-related dimorphisms in murine neuroanatomy have previously been reported using DBM (Spring et al., 2007)), this study used *ex vivo* images with a 32 μm isotropic resolution. At this high spatial resolution, regional analyses were able to reveal distortions/movements between 30–180 μm . Given the lower resolution of our *in vivo* scans (156 μm isotropic), it is unlikely that the subtle effects of gender would influence our data, a conclusion which is supported by the lack of any significant effects of gender in our analysis.

In summary, our results support the utility of longitudinal DBM for the study of *in vivo* multiple timepoint datasets involving mouse models of AD in an automated and exploratory fashion. We were able to identify interesting growth differences between a transgenic APP/PS1 AD mouse model and their wildtype littermates with strong supporting pathophysiological interpretations. The seamless combination of morphological data obtained from this technique with complementary studies, including functional MRI (fMRI), positron emission tomography (PET), quantitative immunohistochemistry, as well as cognitive performance testing, should allow for an improved understanding of complex neuropathological changes and their consequences in multiple diseases of the central nervous system.

3.6 Acknowledgements

The authors would like to thank Drs. Tomas Klason and Fu-Hua Wang at the MR Center of AstraZeneca R&D (AstraZeneca, Södertälje, Sweden) for kindly supplying the MRI and manual segmentation datasets, and Dr. Claude Lepage for valuable discussions regarding the automated image processing pipeline. This work was supported by funds from the Montreal Neurological Institute (B.J.B.). B.J.B. is a Killam Scholar at the Montreal Neurological Institute. J.P.L. is supported by the Canadian Institutes for Health Research. The Mouse Imaging Centre (MICe) acknowledges funding from the Canada Foundation for Innovation and the Ontario Innovation Trust for providing facilities along with The Hospital for Sick Children, as well as operating funds from the Burroughs Wellcome Fund, the Canadian Institutes of Health Research, the National Cancer Institute of Canada - Terry Fox Program Projects, the National Institutes of Health and the Ontario Research and Development Challenge Fund. R.M.H. holds a Canada Research Chair in Imaging.

Table 3.1: Registration schedule

Step	FWHM (μm)	Filter Type	Grid Resolution (μm)
lsq6	5000	Gaussian	NA
lsq6	2000	Gaussian	NA
lsq6	1000	Gradient	NA
lsq6	800	Gaussian	NA
lsq6	500	Gaussian	NA
lsq12	800	Gaussian	NA
lsq12	600	Gradient	NA
lsq12	400	Gaussian	NA
nlin1	800	Gaussian	1000
nlin2	600	Gaussian	800
nlin3	500	Gaussian	700
nlin4	400	Gaussian	600
nlin5	400	Gaussian	400
nlin6	300	Gaussian	400
nlin7	200	Gaussian	300
nlin8	200	Gaussian	200

NA = not applicable

Table 3.2: Main effects of genotype

Region	Symmetry	β_1	t -value	β_1 greater in
<i>Primary somatosensory cortex (jaw region)</i>	right	0.088	4.93	WT
<i>Primary somatosensory cortex (barrel field)</i>	bilateral	0.126	5.11	WT
<i>Retrosplenial and cingulate cortex</i>	medial	0.155	6.58	WT
<i>Piriform cortex</i>	left	0.100	5.03	WT
<i>Olfactory bulb</i>	bilateral	0.126	6.07	WT
<i>Parafoveus</i>	bilateral	0.116	4.87	WT
<i>Anterior commissure</i>	bilateral	0.146	5.83	WT
<i>Corpus callosum</i>	bilateral	0.172	6.20	WT
<i>Cingulum/Dorsal hippocampal commissure</i>	bilateral	0.191	5.69	WT
<i>Cerebellar commissure</i>	bilateral	0.181	5.31	WT
<i>Bed nucleus of stria terminalis</i>	bilateral	-0.170	-8.21	TG
<i>Dorsal superior colliculus</i>	bilateral	-0.116	-5.68	TG
<i>Dorsal periaqueductal gray matter</i>	bilateral	-0.062	-3.56	TG
<i>Stria terminalis</i>	bilateral	-0.175	-4.39	TG
<i>Brachium of superior colliculus</i>	bilateral	-0.097	-3.66	TG
<i>Lateral ventricles</i>	bilateral	-0.137	-5.97	TG
<i>Third ventricle</i>	medial	-0.103	-3.52	TG

β_3 = fixed-effect for genotype

Table 3.3: Interactions between age and genotype

Region	Symmetry	β_3	t -value	β_3 greater in
<i>Lateral entorhinal cortex</i>	left	0.057	3.93	WT
<i>Retrosplenial granular b cortex</i>	medial	0.049	3.75	WT
<i>Hippocampus: CA3 and GrDG</i>	bilateral	0.030	3.95	WT
<i>Flocculus/Paraflocculus</i>	bilateral	0.028	3.44	WT
<i>Primary somatosensory cortex (jaw region)</i>	bilateral	-0.016	-3.88	TG
<i>Primary somatosensory cortex (barrel field)</i>	left	-0.026	-4.09	TG
<i>Retrosplenial and cingulate cortex</i>	right	-0.016	-3.56	TG
<i>Piriform cortex</i>	bilateral	-0.015	-5.02	TG
<i>Dorsolateral hippocampus (CA1 to CA2)</i>	bilateral	-0.032	-4.94	TG
<i>Septofimbrial and septal nucleus</i>	left	-0.017	-6.06	TG
<i>Lateral globus pallidus</i>	right	-0.024	-4.33	TG
<i>Ventral posterolateral thalamic nucleus</i>	left	-0.012	-4.12	TG
<i>Medial vestibular nucleus</i>	bilateral	-0.010	-4.02	TG
<i>Cingulum/Dorsal hippocampal commissure</i>	left	-0.041	-6.43	TG
<i>Cerebellar commissure</i>	right	-0.022	-4.76	TG
<i>Lateral ventricles</i>	bilateral	-0.017	-4.67	TG
<i>Third ventricle</i>	medial	-0.018	-4.49	TG

β_3 = interaction between age and genotype

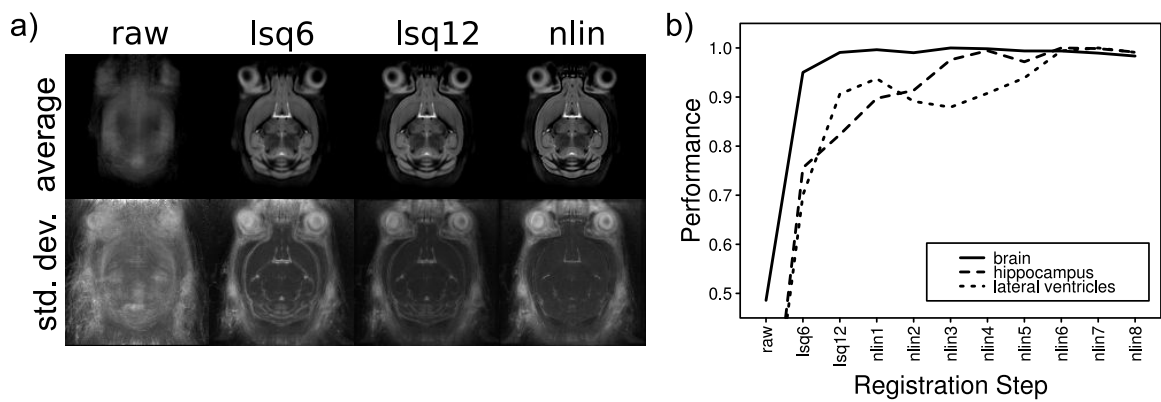


Figure 3.1: Pipeline results for successive stages of reference creation. (a) Average and standard deviation images of the same transverse slice at successive stages of registration. (b) Plots of performance (quantified as voxel overlap) versus registration step for each manually segmented scan. Note that the performance of the algorithm is seen to plateau after the sixth nonlinear registration step.

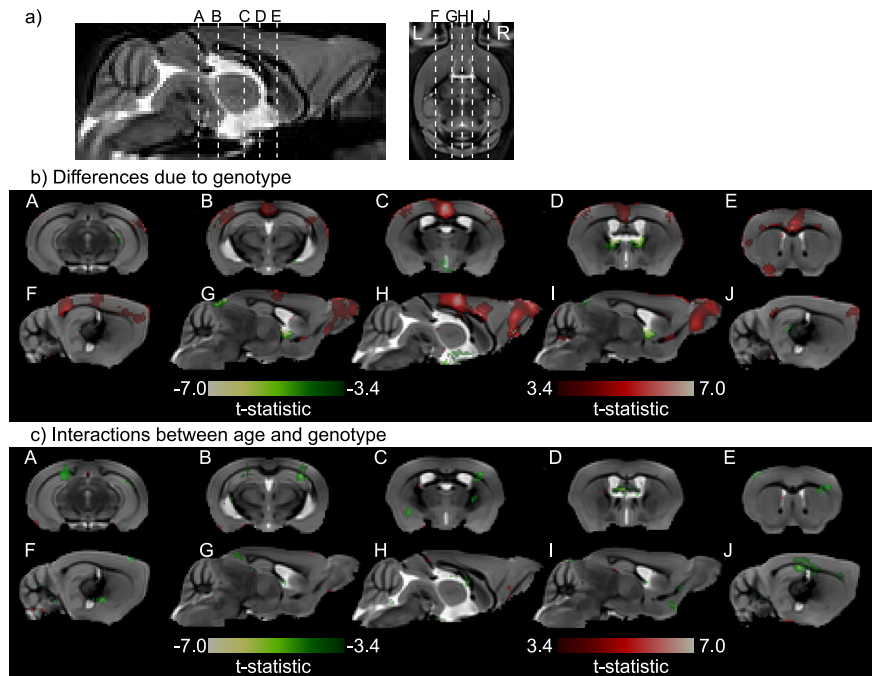


Figure 3.2: Statistical maps demonstrating local volume differences between TG and WT populations. (a) The positions of representative slices throughout the reference space are marked with dashed lines in a mid-sagittal slice for the coronal sections (A-E) and a mid-transverse slice for the sagittal sections (F-J). (b) Regions demonstrating volumetric differences due to genotype across all timepoints. Volumetric expansion and reduction in TG versus WT are shown in green and red, respectively. (c) Regions demonstrating dynamic interactions between age and genotype. Positive and negative interactions are shown in green and red, respectively. All coloured regions are statistically significant by pooled FDR ($q = 0.05$).

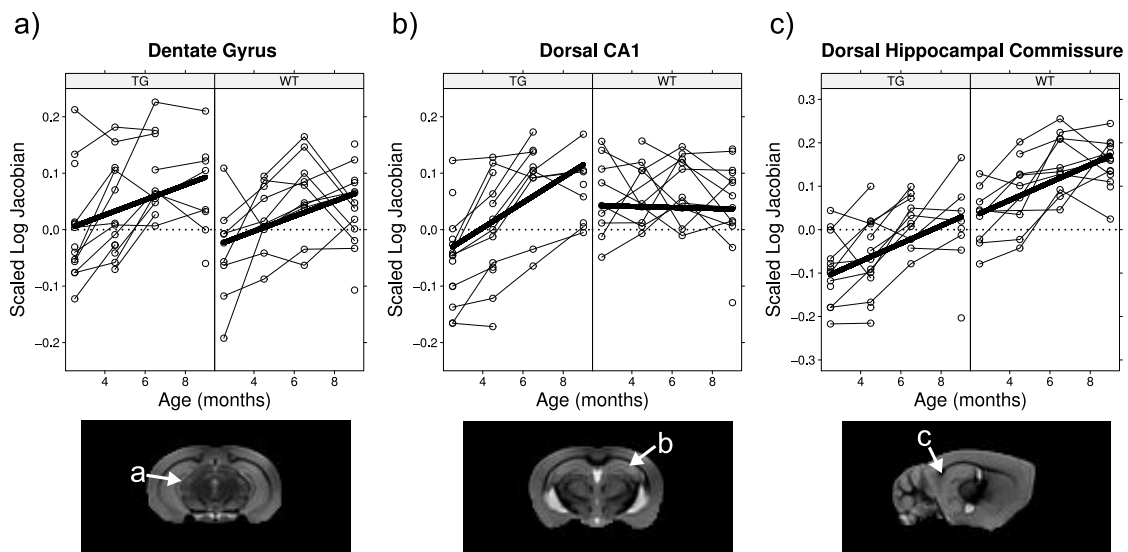


Figure 3.3: Dynamic longitudinal changes illustrated within the hippocampus using the local scaled Jacobian. The voxelwise scaled Jacobians are plotted as open circles. The final predicted model, represented by a thick solid line, includes only significant components of the mixed-effects model, and individual trajectories are connected by thin solid lines. Regions in (a) the left lateral dentate gyrus, (b) the right dorsal hippocampus within CA1, and (c) the left dorsal hippocampal commissure are shown.

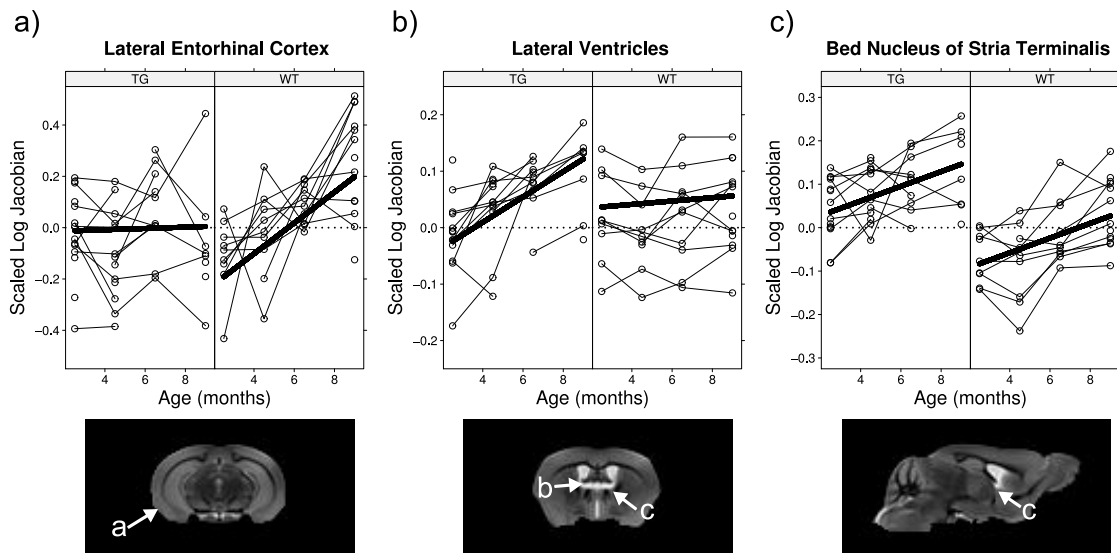


Figure 3.4: Dynamic longitudinal changes illustrated for several regions throughout the brain. The voxelwise scaled Jacobians are plotted as open circles. The final predicted model, represented by a thick solid line, includes only significant components of the mixed-effects model, and individual trajectories are connected by thin solid lines. Regions of (a) the left lateral entorhinal cortex, (b) the lateral ventricles, and (c) the bed nucleus of the stria terminalis are shown.

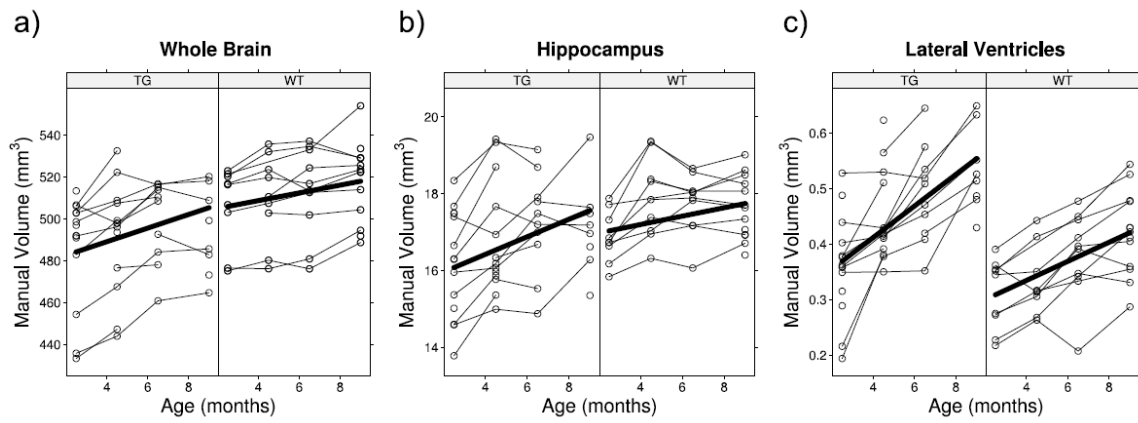


Figure 3.5: Mixed-effects regression plots in three manually segmented neuroanatomical volumes: (a) whole brain, (b) hippocampus, and (c) lateral ventricles. The raw datapoints are plotted as open circles. The final predicted curve is represented by a solid line, and individual trajectories are connected by thin solid lines.

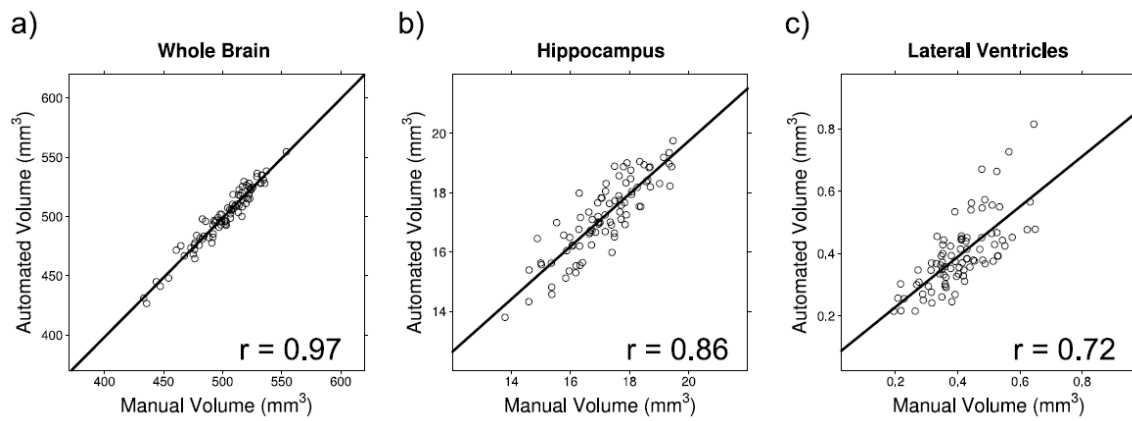


Figure 3.6: Correlation between automated and conventional manual segmentations of (a) whole brain, (b) hippocampus, and (c) lateral ventricles.

Chapter 4

Summary of Findings

The presented thesis examined the utility of an automated image processing technique, DBM, for detecting morphological changes and differences in a longitudinal MRI study of APP/PS1 mice and their wild-type littermates. The results were evaluated against conventional, gold-standard manual segmentations of several neuroanatomical structures of interest. Findings from the study can be summarized as the following:

1. Using both qualitative and quantitative metrics, the unbiased reference creation method of Kovacevic et al. (Kovacevic et al., 2005) was shown to sufficiently improve nonlinear registration prior to longitudinal analysis (Figure 3.1). Visual inspection of average and standard deviation images revealed that anatomical features were both more refined and exhibited less variability with successive registration steps. Performance, quantified as a measure of voxel overlap, was observed to plateau after six nonlinear registration steps to a level of nearly perfect overlap across images.
2. Adaptive spatial filtering was shown to provide improved delineation of morphology in the processed deformation maps due to its ability to better respect anatomical boundaries.
3. Using mixed-model regression, linear age and genotype components, as well as the interaction between genotype with age, were examined. DBM analysis

revealed that each of these components exhibited focal regions of significance throughout the brain (Figure 3.2).

4. With effects of genotype removed, positive linear age-related changes were identified throughout the brain, but particularly in the hippocampus, olfactory bulbs, thalamus, cerebellum, ventricles, and white matter tracts (Figure 3.2b,c).
5. Differences due to genotype, suggesting morphological abnormalities in the TG group, were observed in focal regions of the hippocampus, cortex, olfactory bulbs, stria terminalis, brain stem, ventricles, and certain white matter tracts (e.g. anterior commissure, corpus callosum, dorsal hippocampal commissure, cerebellar commissure) (Figure 3.2d,e and Tables 3.2 & 3.3).
6. Strong correlation between automated and conventional manual volumetry was established across all 86 scans for three segmented neuroanatomical regions: whole brain ($r = 0.97$; $P < 0.0001$), hippocampus ($r = 0.86$; $P < 0.0001$), and lateral ventricles ($r = 0.72$; $P < 0.0001$).

Chapter 5

Conclusions

DBM, in conjunction with unbiased, population-specific reference creation, was found to be an effective, automated technique for examining morphological effects in a longitudinal study of APP/PS1 mice and their wild-type littermates. The presented method is completely data-driven, and therefore can be readily applied to MRI datasets without any *a priori* hypotheses. In conjunction with mixed-effects modelling of local volume (i.e. the Jacobian), morphological patterns due to differences in genetic background, and longitudinal, age-related change were detected in an exploratory fashion throughout the brain, confirming findings from literature, as well as revealing novel anatomical regions of interest.

Chapter 6

Future Work

The described method of nonlinear reference creation and subsequent DBM analysis has been shown to achieve excellent results on a longitudinal MRI dataset involving both transgenic and wild-type mice. However, there are clearly ways in which the analysis could be improved.

1. While the focal changes/differences found in this study appear to be well-supported by literature, the only way to truly confirm our findings would be to use microscopic neuropathological examination, which would include study by histochemistry and immunohistochemistry.
2. A validation study with multiple raters and multiple segmented neuroanatomical structures using this dataset would allow for true quantification of inter- and intra-rater reliability measures as related to the robustness of the registration strategy to longitudinal datasets.
3. The reference creation strategy employed confers equal morphological weight to each input MRI scan in the resulting population average. There are two major drawbacks to the current strategy. First, the created reference space may be anatomically weighted toward the more represented subpopulations in the input dataset. Second, the pairwise alignment strategy may be overly computationally intensive for large MRI datasets particularly as they become increasingly available as a result of high-throughput imaging (e.g. Nieman et al., 2005b)

and multicenter studies. In *Big O* notation, the complexity of the algorithm is $O(n^2)$, where n is the amount of input data (i.e. the number of MR images in the dataset). This quadratic dependence on the input data may be inefficient and alternative reference creation strategies, that may be better optimized for these purposes, should be explored. Furthermore, it may be worth investigating the performance of the nonlinear registration method used (Collins et al., 1995) against other warping methods that may take into account fluid and elastic modeling constraints (Christensen and Johnson, 2001; Davatzikos et al., 2001; Leow et al., 2006).

4. The adaptive filtering technique, first described by Studholme et al. (Studholme et al., 2003), and implemented here, was shown to provide improved delineation of features of interest. However, alternative anisotropic techniques should also be investigated.
5. In this study, the Jacobian determinant was assessed at each voxel as a means of examining local volumetric effects across the entire dataset. This measure was chosen because it provides the simplest and most readily interpretable term that can be extracted from the local deformation vector. The effect of higher-order terms of the Jacobian matrix that include vector direction or strain should be investigated as they can provide improved characterization of neuroanatomical effects, as well as more statistical power (Thompson et al., 2007).
6. The mixed-effects regression technique employed in this study required normally distributed observations. In order to obviate the need for such an assumption, the possibility of using nonparametric models to characterize longitudinal DBM-based changes should be explored.
7. Future studies should confirm and look to further quantify the longitudinal morphological changes reported in the APP/PS1 and their WT littermates. Greater temporal resolution, as the result of more scanned timepoints, and larger study designs would allow for improved curvilinear descriptions of age-related local structural change.
8. While the longitudinal DBM method was demonstrated here for an MRI dataset of double transgenic APP/PS1 mice, the generalizability of this method to the study of other murine models of AD, and to other models of CNS disease should be explored.

Bibliography

- Ali, A. A., Dale, A. M., Badea, A., Johnson, G. A., August 2005. Automated segmentation of neuroanatomical structures in multispectral MR microscopy of the mouse brain. *NeuroImage* 27 (2), 425–435.
- Anderson, V. C., Litvack, Z. N., Kaye, J. A., December 2005. Magnetic resonance approaches to brain aging and Alzheimer disease-associated neuropathology. *Top Magn Reson Imaging* 16 (6), 439–452.
- Andreoli, T. E., Carpenter, C. C. J., Griggs, R. C., Benjamin, I., March 2007. Andreoli and Carpenter’s *Cecil Essentials of Medicine*, 7th Edition. Saunders.
- Ashburner, J., Csernansky, J. G., Davatzikos, C., Fox, N. C., Frisoni, G. B., Thompson, P. M., February 2003. Computer-assisted imaging to assess brain structure in healthy and diseased brains. *Lancet Neurol* 2 (2), 79–88.
- Ashburner, J., Friston, K. J., June 2000. Voxel-based morphometry—the methods. *NeuroImage* 11 (6 Pt 1), 805–821.
- Ashburner, J., Friston, K. J., December 2001. Why voxel-based morphometry should be used. *NeuroImage* 14 (6), 1238–1243.
- Ashburner, J., Hutton, C., Frackowiak, R., Johnsrude, I., Price, C., Friston, K., 1998. Identifying global anatomical differences: deformation-based morphometry. *Hum Brain Mapp* 6 (5-6), 348–357.
- Attems, J., Lintner, F., Jellinger, K. A., April 2005. Olfactory involvement in aging and Alzheimer’s disease: an autopsy study. *J Alzheimers Dis* 7 (2).
- Aucoin, J. S., Jiang, P., Aznavour, N., Tong, X. K., Buttini, M., Descarries, L., Hamel, E., 2005. Selective cholinergic denervation, independent from oxidative stress, in a mouse model of Alzheimer’s disease. *Neuroscience* 132 (1), 73–86.

- Badea, A., Ali-Sharief, A. A., Johnson, G. A., September 2007. Morphometric analysis of the C57BL/6J mouse brain. *NeuroImage* 37 (3), 683–693.
- Bajcsy, R., Kovacic, S., April 1989. Multiresolution elastic matching. *Computer Vision, Graphics, and Image Processing* 46 (1), 1–21.
- Barnes, J., Foster, J., Fox, N. C., June 2007. Structural magnetic resonance imaging-derived biomarkers for Alzheimer’s disease. *Biomarkers in Medicine* 1 (1), 79–92.
- Bookstein, F. L., April 1997. Landmark methods for forms without landmarks: morphometrics of group differences in outline shape. *Med Image Anal* 1 (3), 225–243.
- Bookstein, F. L., December 2001. Voxel-based morphometry should not be used with imperfectly registered images. *NeuroImage* 14 (6), 1454–1462.
- Borchelt, D. R., Ratovitski, T., van Lare, J., Lee, M. K., Gonzales, V., Jenkins, N. A., Copeland, N. G., Price, D. L., Sisodia, S. S., October 1997. Accelerated amyloid deposition in the brains of transgenic mice coexpressing mutant presenilin 1 and amyloid precursor proteins. *Neuron* 19 (4), 939–945.
- Braak, H., Braak, E., 1991. Neuropathological staging of Alzheimer-related changes. *Acta Neuropathol (Berl)* 82 (4), 239–259.
- Bradley, K. M., Bydder, G. M., Budge, M. M., Hajnal, J. V., White, S. J., Ripley, B. D., Smith, A. D., June 2002. Serial brain MRI at 3-6 month intervals as a surrogate marker for Alzheimer’s disease. *Br J Radiol* 75 (894), 506–513.
- Cao, J., Worsley, K. J., 1999. The detection of local shape changes via the geometry of Hotelling’s T^2 fields. *The Annals of Statistics* 27 (3), 925–942.
- Castellanos, F. X., Lee, P. P., Sharp, W., Jeffries, N. O., Greenstein, D. K., Clasen, L. S., Blumenthal, J. D., James, R. S., Ebens, C. L., Walter, J. M., Zijdenbos, A., Evans, A. C., Giedd, J. N., Rapoport, J. L., October 2002. Developmental trajectories of brain volume abnormalities in children and adolescents with attention-deficit/hyperactivity disorder. *JAMA* 288 (14), 1740–1748.
- Chan, E., Kovacevc, N., Ho, S. K., Henkelman, R. M., Henderson, J. T., January 2007. Development of a high resolution three-dimensional surgical atlas of the murine head for strains 129S1/SvImJ and C57Bl/6J using magnetic resonance imaging and micro-computed tomography. *Neuroscience* 144 (2), 604–615.

- Chen, X. J., Kovacevic, N., Lobaugh, N. J., Sled, J. G., Henkelman, R. M., Henderson, J. T., January 2006. Neuroanatomical differences between mouse strains as shown by high-resolution 3D MRI. *NeuroImage* 29 (1), 99–105.
- Christensen, G. E., Johnson, H. J., 2001. Consistent image registration. *Medical Imaging, IEEE Transactions on* 20 (7), 568–582.
- Christensen, G. E., Johnson, H. J., Vannier, M. W., August 2006. Synthesizing average 3D anatomical shapes. *NeuroImage* 32 (1), 146–158.
- Chung, M. K., Worsley, K. J., Paus, T., Cherif, C., Collins, D. L., Giedd, J. N., Rapoport, J. L., Evans, A. C., September 2001. A unified statistical approach to deformation-based morphometry. *NeuroImage* 14 (3), 595–606.
- Cocosco, C. A., Zijdenbos, A. P., Evans, A. C., December 2003. A fully automatic and robust brain MRI tissue classification method. *Med Image Anal* 7 (4), 513–527.
- Collins, D. L., Neelin, P., Peters, T. M., Evans, A. C., 1994. Automatic 3D intersubject registration of MR volumetric data in standardized Talairach space. *J Comput Assist Tomogr* 18 (2), 192–205.
- Collins, L. D., Holmes, C. J., Peters, T. M., Evans, A. C., 1995. Automatic 3-D model-based neuroanatomical segmentation. *Human Brain Mapping* 3 (3), 190–208.
- Corder, E. H., Saunders, A. M., Strittmatter, W. J., Schmechel, D. E., Gaskell, P. C., Small, G. W., Roses, A. D., Haines, J. L., Pericak-Vance, M. A., August 1993. Gene dose of apolipoprotein E type 4 allele and the risk of Alzheimer’s disease in late onset families. *Science* 261 (5123), 921–923.
- Crum, W. R., Scahill, R. I., Fox, N. C., May 2001. Automated hippocampal segmentation by regional fluid registration of serial MRI: validation and application in Alzheimer’s disease. *NeuroImage* 13 (5), 847–855.
- Dale, A. M., Fischl, B., Sereno, M. I., February 1999. Cortical surface-based analysis. I. segmentation and surface reconstruction. *NeuroImage* 9 (2), 179–194.
- Davatzikos, C., Genc, A., Xu, D., Resnick, S. M., December 2001. Voxel-based morphometry using the RAVENS maps: methods and validation using simulated longitudinal atrophy. *NeuroImage* 14 (6), 1361–1369.

- Davatzikos, C., Vaillant, M., Resnick, S. M., Prince, J. L., Letovsky, S., Bryan, R. N., 1996. A computerized approach for morphological analysis of the corpus callosum. *J Comput Assist Tomogr* 20 (1), 88–97.
- Delatour, B., Guegan, M., Volk, A., Dhenain, M., June 2006. In vivo MRI and histological evaluation of brain atrophy in APP/PS1 transgenic mice. *Neurobiology of Aging* 27 (6), 835–847.
- Dhenain, M., Ruffins, S. W., Jacobs, R. E., April 2001. Three-dimensional digital mouse atlas using high-resolution MRI. *Dev Biol* 232 (2), 458–470.
- Doody, R. S., Stevens, J. C., Beck, C., Dubinsky, R. M., Kaye, J. A., Gwyther, L., Mohs, R. C., Thal, L. J., Whitehouse, P. J., DeKosky, S. T., Cummings, J. L., May 2001. Practice parameter: management of dementia (an evidence-based review). report of the quality standards subcommittee of the american academy of neurology. *Neurology* 56 (9), 1154–1166.
- Duda, R. O., Hart, P. E., Stork, D. G., November 2000. *Pattern Classification* (2nd Edition). Wiley-Interscience.
- Evans, A. C., December 2005. Large-scale morphometric analysis of neuroanatomy and neuropathology. *Anat Embryol (Berl)* 210 (5-6), 439–446.
- Evans, A. C. a., March 2006. The NIH MRI study of normal brain development. *NeuroImage* 30 (1), 184–202.
- Feldman, H. H., Jacova, C., Robillard, A., Garcia, A., Chow, T., Borrie, M., Schipper, H. M., Blair, M., Kertesz, A., Chertkow, H., March 2008. Diagnosis and treatment of dementia: 2. diagnosis. *CMAJ* 178 (7), 825–836.
- Ferrarini, L., Palm, W. M., Olofsen, H., van Buchem, M. A., Reiber, J. H., Admiraal-Behloul, F., September 2006. Shape differences of the brain ventricles in Alzheimer’s disease. *NeuroImage* 32 (3), 1060–1069.
- Fischl, B., Salat, D. H., Busa, E., Albert, M., Dieterich, M., Haselgrove, C., van der Kouwe, A., Killiany, R., Kennedy, D., Klaveness, S., Montillo, A., Makris, N., Rosen, B., Dale, A. M., January 2002. Whole brain segmentation: automated labeling of neuroanatomical structures in the human brain. *Neuron* 33 (3), 341–355.

- Folstein, M. F., Folstein, S. E., McHugh, P. R., November 1975. "mini-mental state". a practical method for grading the cognitive state of patients for the clinician. *J Psychiatr Res* 12 (3), 189–198.
- Fox, N. C., Crum, W. R., Scahill, R. I., Stevens, J. M., Janssen, J. C., Rossor, M. N., July 2001. Imaging of onset and progression of Alzheimer's disease with voxel-compression mapping of serial magnetic resonance images. *Lancet* 358 (9277), 201–205.
- Freedman, M., Leach, L., Kaplan, E., Winocur, G., Shulman, K., Delis, D. C., February 1994. *Clock Drawing: A Neuropsychological Analysis*, 1st Edition. Oxford University Press, USA.
- Games, D., Buttini, M., Kobayashi, D., Schenk, D., Seubert, P., 2006. Mice as models: transgenic approaches and Alzheimer's disease. *J Alzheimers Dis* 9 (3 Suppl), 133–149.
- Genovese, C. R., Lazar, N. A., Nichols, T., April 2002. Thresholding of statistical maps in functional neuroimaging using the false discovery rate. *NeuroImage* 15 (4), 870–878.
- Goate, A., Chartier-Harlin, M.-C., Mullan, M., Brown, J., Crawford, F., Fidani, L., Giuffra, L., Haynes, A., Irving, N., James, L., Mant, R., Newton, P., Rooke, K., Roques, P., Talbot, C., Pericak-Vance, M., Roses, A., Williamson, R., Rossor, M., Owen, M., Hardy, J., February 1991. Segregation of a missense mutation in the amyloid precursor protein gene with familial Alzheimer's disease. *Nature* 349 (6311), 704–706.
- Good, C. D., Johnsrude, I. S., Ashburner, J., Henson, R. N., Friston, K. J., Frackowiak, R. S., July 2001. A voxel-based morphometric study of ageing in 465 normal adult human brains. *NeuroImage* 14 (1 Pt 1), 21–36.
- Good, C. D., Scahill, R. I., Fox, N. C., Ashburner, J., Friston, K. J., Chan, D., Crum, W. R., Rossor, M. N., Frackowiak, R. S., September 2002. Automatic differentiation of anatomical patterns in the human brain: validation with studies of degenerative dementias. *NeuroImage* 17 (1), 29–46.
- Gordon, M. N., Holcomb, L. A., Jantzen, P. T., DiCarlo, G., Wilcock, D., Boyett, K. W., Connor, K., Melachrinou, J., O'Callaghan, J. P., Morgan, D., February

2002. Time course of the development of Alzheimer-like pathology in the doubly transgenic PS1+APP mouse. *Exp Neurol* 173 (2), 183–195.
- Gordon, M. N., King, D. L., Diamond, D. M., Jantzen, P. T., Boyett, K. V., Hope, C. E., Hatcher, J. M., DiCarlo, G., Gottschall, W. P., Morgan, D., Arendash, G. W., 2001. Correlation between cognitive deficits and Abeta deposits in transgenic APP+PS1 mice. *Neurobiol Aging* 22 (3), 377–385.
- Grenander, U., Miller, M. I., 1998. Computational anatomy: an emerging discipline. *Q. Appl. Math.* LVI (4), 617–694.
- Hampel, H., Teipel, S. J., Alexander, G. E., Horwitz, B., Teichberg, D., Schapiro, M. B., Rapoport, S. I., February 1998. Corpus callosum atrophy is a possible indicator of region- and cell type-specific neuronal degeneration in Alzheimer disease: a magnetic resonance imaging analysis. *Arch Neurol* 55 (2), 193–198.
- Hebert, L. E., Scherr, P. A., Bienias, J. L., Bennett, D. A., Evans, D. A., August 2003. Alzheimer disease in the US population: prevalence estimates using the 2000 census. *Arch Neurol* 60 (8), 1119–1122.
- Heckemann, R. A. A., Hajnal, J. V. V., Aljabar, P., Rueckert, D., Hammers, A., July 2006. Automatic anatomical brain MRI segmentation combining label propagation and decision fusion. *NeuroImage* 33 (1), 115–126.
- Higgins, G. A., Jacobsen, H., September 2003. Transgenic mouse models of Alzheimer's disease: phenotype and application. *Behav Pharmacol* 14 (5-6), 419–438.
- Holcomb, L., Gordon, M. N., McGowan, E., Yu, X., Benkovic, S., Jantzen, P., Wright, K., Saad, I., Mueller, R., Morgan, D., Sanders, S., Zehr, C., O'Campo, K., Hardy, J., Prada, C. M., Eckman, C., Younkin, S., Hsiao, K., Duff, K., January 1998. Accelerated Alzheimer-type phenotype in transgenic mice carrying both mutant amyloid precursor protein and presenilin 1 transgenes. *Nat Med* 4 (1), 97–100.
- Holcomb, L. A., Gordon, M. N., Jantzen, P., Hsiao, K., Duff, K., Morgan, D., May 1999. Behavioral changes in transgenic mice expressing both amyloid precursor protein and presenilin-1 mutations: lack of association with amyloid deposits. *Behav Genet* 29 (3), 177–185.

- Holmes, C. J., Hoge, R., Collins, L., Woods, R., Toga, A. W., Evans, A. C., 1998. Enhancement of MR images using registration for signal averaging. *J Comput Assist Tomogr* 22 (2), 324–333.
- Howlett, D. R., Richardson, J. C., Austin, A., Parsons, A. A., Bate, S. T., Davies, C. D., Gonzalez, I. M., August 2004. Cognitive correlates of a[beta] deposition in male and female mice bearing amyloid precursor protein and presenilin-1 mutant transgenes. *Brain Research* 1017 (1-2), 130–136.
- Hsia, A. Y., Masliah, E., Mcconlogue, L., Yu, G.-Q., Tatsuno, G., Hu, K., Kholodenko, D., Malenka, R. C., Nicoll, R. A., Mucke, L., March 1999. Plaque-independent disruption of neural circuits in Alzheimer's disease mouse models. *PNAS* 96 (6), 3228–3233.
- Hsiao, K., Chapman, P., Nilsen, S., Eckman, C., Harigaya, Y., Younkin, S., Yang, F., Cole, G., October 1996. Correlative memory deficits, abeta elevation, and amyloid plaques in transgenic mice. *Science* 274 (5284), 99–102.
- Hsu, Y.-Y., Schuff, N., Du, A.-T., Mark, K., Zhu, X., Hardin, D., Weiner, M. W., 2002. Comparison of automated and manual MRI volumetry of hippocampus in normal aging and dementia. *Journal of Magnetic Resonance Imaging* 16 (3), 305–310.
- Iseki, E., Matsushita, M., Kosaka, K., Kondo, H., Ishii, T., Amano, N., 1989. Distribution and morphology of brain stem plaques in Alzheimer's disease. *Acta Neuropathol (Berl)* 78 (2), 131–136.
- Jack, C. R., Marjanska, M., Wengenack, T. M., Reyes, D. A., Curran, G. L., Lin, J., Preboske, G. M., Poduslo, J. F., Garwood, M., February 2007. Magnetic resonance imaging of Alzheimer's pathology in the brains of living transgenic mice: a new tool in Alzheimer's disease research. *Neuroscientist* 13 (1), 38–48.
- Janke, A. L., de Zubicaray, G., Rose, S. E., Griffin, M., Chalk, J. B., Galloway, G. J., October 2001. 4D deformation modeling of cortical disease progression in Alzheimer's dementia. *Magn Reson Med* 46 (4), 661–666.
- Kochunov, P., Lancaster, J. L., Thompson, P., Woods, R., Mazziotta, J., Hardies, J., Fox, P., 2001. Regional spatial normalization: toward an optimal target. *J Comput Assist Tomogr* 25 (5), 805–816.

- Kovacevic, N., Henderson, J. T., Chan, E., Lifshitz, N., Bishop, J., Evans, A. C., Henkelman, R. M., Chen, X. J., May 2005. A three-dimensional MRI atlas of the mouse brain with estimates of the average and variability. *Cereb Cortex* 15 (5), 639–645.
- Kovacevic, N., Lobaugh, N. J., Bronskill, M. J., Levine, B., Feinstein, A., Black, S. E., November 2002. A robust method for extraction and automatic segmentation of brain images. *NeuroImage* 17 (3), 1087–1100.
- Kurt, M. A., Davies, D. C., Kidd, M., Duff, K., Rolph, S. C., Jennings, K. H., Howlett, D. R., September 2001. Neurodegenerative changes associated with beta-amyloid deposition in the brains of mice carrying mutant amyloid precursor protein and mutant presenilin-1 transgenes. *Exp Neurol* 171 (1), 59–71.
- Larner, A. J., Doran, M., February 2006. Clinical phenotypic heterogeneity of Alzheimer's disease associated with mutations of the presenilin-1 gene. *J Neurol* 253 (2), 139–158.
- Larson, J., Lynch, G., Games, D., Seubert, P., September 1999. Alterations in synaptic transmission and long-term potentiation in hippocampal slices from young and aged PDAPP mice. *Brain Res* 840 (1-2), 23–35.
- Lavebratt, C., Trifunovski, A., Persson, A. S., Wang, F. H., Klason, T., Ohman, I., Josephsson, A., Olson, L., Spenger, C., Schalling, M., November 2006. Carbamazepine protects against megencephaly and abnormal expression of BDNF and Nogo signaling components in the mceph/mceph mouse. *Neurobiol Dis* 24 (2), 374–383.
- Leow, A. D. D., Klunder, A. D. D., Jack, C. R. R., Toga, A. W. W., Dale, A. M. M., Bernstein, M. A. A., Britson, P. J. J., Gunter, J. L. L., Ward, C. P. P., Whitwell, J. L. L., Borowski, B. J. J., Fleisher, A. S. S., Fox, N. C. C., Harvey, D., Kornak, J., Schuff, N., Studholme, C., Alexander, G. E. E., Weiner, M. W. W., Thompson, P. M. M. a., February 2006. Longitudinal stability of MRI for mapping brain change using tensor-based morphometry. *NeuroImage*.
- Lerch, J. P., Evans, A. C., January 2005. Cortical thickness analysis examined through power analysis and a population simulation. *NeuroImage* 24 (1), 163–173.

- Lerch, J. P., Pruessner, J. C., Zijdenbos, A., Hampel, H., Teipel, S. J., Evans, A. C., July 2005. Focal decline of cortical thickness in Alzheimer's disease identified by computational neuroanatomy. *Cereb Cortex* 15 (7), 995–1001.
- Lerch, J. P. P., Pruessner, J., Zijdenbos, A. P. P., Collins, D. L. L., Teipel, S. J. J., Hampel, H., Evans, A. C. C., November 2006. Automated cortical thickness measurements from MRI can accurately separate Alzheimer's patients from normal elderly controls. *Neurobiol Aging*.
- Levy-Lahad, E., Wasco, W., Poorkaj, P., Romano, D. M., Oshima, J., Pettingell, W. H., Yu, C. E., Jondro, P. D., Schmidt, S. D., Wang, K., August 1995. Candidate gene for the chromosome 1 familial Alzheimer's disease locus. *Science* 269 (5226), 973–977.
- Ma, Y., Hof, P. R., Grant, S. C., Blackband, S. J., Bennett, R., Slatest, L., McGuigan, M. D., Benveniste, H., 2005. A three-dimensional digital atlas database of the adult C57BL/6J mouse brain by magnetic resonance microscopy. *Neuroscience* 135 (4), 1203–1215.
- MacDonald, D., Kabani, N., Avis, D., Evans, A. C., September 2000. Automated 3-d extraction of inner and outer surfaces of cerebral cortex from MRI. *NeuroImage* 12 (3), 340–356.
- MacKenzie-Graham, A., Lee, E. F., Dinov, I. D., Bota, M., Shattuck, D. W., Ruffins, S., Yuan, H., Konstantinidis, F., Pitiot, A., Ding, Y., Hu, G., Jacobs, R. E., Toga, A. W., February 2004. A multimodal, multidimensional atlas of the C57BL/6J mouse brain. *J Anat* 204 (2), 93–102.
- Mazziotta, J., Toga, A., Evans, A., Fox, P., Lancaster, J., Zilles, K., Woods, R., Paus, T., Simpson, G., Pike, B., Holmes, C., Collins, L., Thompson, P., MacDonald, D., Iacoboni, M., Schormann, T., Amunts, K., Palomero-Gallagher, N., Geyer, S., Parsons, L., Narr, K., Kabani, N., Le Goualher, G., Boomsma, D., Cannon, T., Kawashima, R., Mazoyer, B., August 2001. A probabilistic atlas and reference system for the human brain: International Consortium for Brain Mapping (ICBM). *Philos Trans R Soc Lond B Biol Sci* 356 (1412), 1293–1322.
- Mazziotta, J. C., Toga, A. W., Evans, A., Fox, P., Lancaster, J., June 1995. A probabilistic atlas of the human brain: Theory and rationale for its development :

- The International Consortium for Brain Mapping (ICBM). *NeuroImage* 2 (2, Part 1), 89–101.
- Mcconville, P., Moody, J. B., Moffat, B. A., August 2005. High-throughput magnetic resonance imaging in mice for phenotyping and therapeutic evaluation. *Current Opinion in Chemical Biology* 9 (4), 413–420.
- McGowan, E., Sanders, S., Iwatsubo, T., Takeuchi, A., Saido, T., Zehr, C., Yu, X., Uljon, S., Wang, R., Mann, D., Dickson, D., Duff, K., August 1999. Amyloid phenotype characterization of transgenic mice overexpressing both mutant amyloid precursor protein and mutant presenilin 1 transgenes. *Neurobiol Dis* 6 (4), 231–244.
- Mount, C., Downton, C., July 2006. Alzheimer disease: progress or profit? *Nature Medicine* 12 (7), 780–784.
- Mucke, L., Masliah, E., Yu, G.-Q., Mallory, M., Rockenstein, E. M., Tatsuno, G., Hu, K., Kholodenko, D., Johnson-Wood, K., Mcconlogue, L., June 2000. High-level neuronal expression of abeta 1-42 in wild-type human amyloid protein precursor transgenic mice: Synaptotoxicity without plaque formation. *J. Neurosci.* 20 (11), 4050–4058.
- Mueller, S. G. G., Weiner, M. W. W., Thal, L. J. J., Petersen, R. C. C., Jack, C. R. R., Jagust, W., Trojanowski, J. Q. Q., Toga, A. W. W., Beckett, L., July 2005. Ways toward an early diagnosis in Alzheimer's disease: The Alzheimer's Disease Neuroimaging Initiative (ADNI). *Alzheimers Dement* 1 (1), 55–66.
- Mufson, E. J., Cochran, E., Benzing, W., Kordower, J. H., 1993. Galaninergetic innervation of the cholinergic vertical limb of the diagonal band (Ch2) and bed nucleus of the stria terminalis in aging, Alzheimer's disease and Down's syndrome. *Dementia* 4 (5), 237–250.
- Mullan, M., Crawford, F., Axelman, K., Houlden, H., Lilius, L., Winblad, B., Lannfelt, L., August 1992. A pathogenic mutation for probable Alzheimer's disease in the APP gene at the N-terminus of beta-amyloid. *Nat Genet* 1 (5), 345–347.
- Nieman, B. J., Bock, N. A., Bishop, J., Chen, X. J., Sled, J. G., Rossant, J., Henkelman, R. M., November 2005a. Magnetic resonance imaging for detection and analysis of mouse phenotypes. *NMR Biomed* 18 (7), 447–468.

- Nieman, B. J., Bock, N. A., Bishop, J., Sled, J. G., Josette Chen, X., Mark Henkelman, R., September 2005b. Fast spin-echo for multiple mouse magnetic resonance phenotyping. *Magn Reson Med* 54 (3), 532–537.
- Nieman, B. J., Flenniken, A. M., Adamson, S. L., Henkelman, R. M., Sled, J. G., January 2006. Anatomical phenotyping in the brain and skull of a mutant mouse by magnetic resonance imaging and computed tomography. *Physiol Genomics* 24 (2), 154–162.
- Nishimura, D. G., April 1996. Principles of magnetic resonance imaging. Stanford University.
- Niwa, K., Kazama, K., Younkin, S. G., Carlson, G. A., Iadecola, C., February 2002. Alterations in cerebral blood flow and glucose utilization in mice overexpressing the amyloid precursor protein. *Neurobiol Dis* 9 (1), 61–68.
- Oberg, J., Spenger, C., Wang, F.-H. H., Andersson, A., Westman, E., Skoglund, P., Sunnemark, D., Norinder, U., Klason, T., Wahlund, L.-O. O., Lindberg, M., April 2007. Age related changes in brain metabolites observed by (1)H MRS in APP/PS1 mice. *Neurobiol Aging*.
- Ono, M., Kubik, S., Abarnathey, C. D., 1990. Atlas of the Cerebral Sulci. Thieme Medical Publishers.
- Palop, J. J., Chin, J., Bien-Ly, N., Massaro, C., Yeung, B. Z., Yu, G. Q., Mucke, L., October 2005. Vulnerability of dentate granule cells to disruption of arc expression in human amyloid precursor protein transgenic mice. *J Neurosci* 25 (42), 9686–9693.
- Palop, J. J., Jones, B., Kekoni, L., Chin, J., Yu, G. Q., Raber, J., Masliah, E., Mucke, L., August 2003. Neuronal depletion of calcium-dependent proteins in the dentate gyrus is tightly linked to Alzheimer's disease-related cognitive deficits. *Proc Natl Acad Sci USA* 100 (16), 9572–9577.
- Paxinos, G., Franklin, K. B. J., August 2001. The Mouse Brain in Stereotaxic Coordinates, Second Edition. Academic Press.
- Pinheiro, J. C., Bates, D. M., April 2002. Mixed Effects Models in S and S-Plus. Springer.

- Reddick, W. E., Glass, J. O., Cook, E. N., Elkin, T. D., Deaton, R. J., December 1997. Automated segmentation and classification of multispectral magnetic resonance images of brain using artificial neural networks. *IEEE Trans Med Imaging* 16 (6), 911–918.
- Redwine, J. M., Kosofsky, B., Jacobs, R. E., Games, D., Reilly, J. F., Morrison, J. H., Young, W. G., Bloom, F. E., February 2003. Dentate gyrus volume is reduced before onset of plaque formation in PDAPP mice: a magnetic resonance microscopy and stereologic analysis. *Proc Natl Acad Sci USA* 100 (3), 1381–1386.
- Reilly, J. F., Games, D., Rydel, R. E., Freedman, S., Schenk, D., Young, W. G., Morrison, J. H., Bloom, F. E., April 2003. Amyloid deposition in the hippocampus and entorhinal cortex: Quantitative analysis of a transgenic mouse model. *PNAS* 100 (8), 4837–4842.
- Resnick, S. M., Pham, D. L., Kraut, M. A., Zonderman, A. B., Davatzikos, C., April 2003. Longitudinal magnetic resonance imaging studies of older adults: A shrinking brain. *J. Neurosci.* 23 (8), 3295–3301.
- Robbins, S., Evans, A. C., Collins, L. D., Whitesides, S., September 2004. Tuning and comparing spatial normalization methods. *Medical Image Analysis* 8 (3), 311–323.
- Rogaeva, E., Meng, Y., Lee, J. H. H., Gu, Y., Kawarai, T., Zou, F., Katayama, T., Baldwin, C. T. T., Cheng, R., Hasegawa, H., Chen, F., Shibata, N., Lunetta, K. L. L., Pardossi-Piquard, R., Bohm, C., Wakutani, Y., Cupples, L. A. A., Cuenco, K. T. T., Green, R. C. C., Pinessi, L., Rainero, I., Sorbi, S., Bruni, A., Duara, R., Friedland, R. P. P., Inzelberg, R., Hampe, W., Bujo, H., Song, Y.-Q. Q., Andersen, O. M. M., Willnow, T. E. E., Graff-Radford, N., Petersen, R. C. C., Dickson, D., Der, S. D. D., Fraser, P. E. E., Schmitt-Ulms, G., Younkin, S., Mayeux, R., Farrer, L. A. A., St George-Hyslop, P., January 2007. The neuronal sortilin-related receptor SORL1 is genetically associated with Alzheimer disease. *Nat Genet.*
- Rohlfing, T., Brandt, R., Menzel, R., Maurer, C. R., April 2004. Evaluation of atlas selection strategies for atlas-based image segmentation with application to confocal microscopy images of bee brains. *NeuroImage* 21 (4), 1428–1442.
- Schellenberg, G., Bird, T., Wijsman, E., Orr, H., Anderson, L., Nemens, E., White, J., Bonycastle, L., Weber, J., Alonso, M., Et, A., October 1992. Genetic link-

- age evidence for a familial Alzheimer's disease locus on chromosome 14. *Science* 258 (5082), 668–671.
- Schwarz, A. J., Danckaert, A., Reese, T., Gozzi, A., Paxinos, G., Watson, C., Merlo-Pich, E. V., Bifone, A., August 2006. A stereotaxic MRI template set for the rat brain with tissue class distribution maps and co-registered anatomical atlas: Application to pharmacological MRI. *NeuroImage* 32 (2), 538–550.
- Selkoe, D. J., April 2001. Alzheimer's disease: genes, proteins, and therapy. *Physiol Rev* 81 (2), 741–766.
- Shaw, P., Eckstrand, K., Sharp, W., Blumenthal, J., Lerch, J. P., Greenstein, D., Clasen, L., Evans, A., Giedd, J., Rapoport, J. L., December 2007. From the cover: Attention-deficit/hyperactivity disorder is characterized by a delay in cortical maturation. *Proc Natl Acad Sci USA* 104 (49), 19649–19654.
- Shaw, P., Greenstein, D., Lerch, J., Clasen, L., Lenroot, R., Gogtay, N., Evans, A., Rapoport, J., Giedd, J., March 2006. Intellectual ability and cortical development in children and adolescents. *Nature* 440 (7084), 676–679.
- Sherrington, R., Rogaev, E. I., Liang, Y., Rogaeva, E. A., Levesque, G., Ikeda, M., Chi, H., Lin, C., Li, G., Holman, K., June 1995. Cloning of a gene bearing missense mutations in early-onset familial Alzheimer's disease. *Nature* 375 (6534), 754–760.
- Singh, V., Chertkow, H., Lerch, J. P., Evans, A. C., Dorr, A. E., Kabani, N. J., November 2006. Spatial patterns of cortical thinning in mild cognitive impairment and alzheimer's disease. *Brain* 129 (Pt 11), 2885–2893.
- Sled, J. G., Zijdenbos, A. P., Evans, A. C., 1998. A nonparametric method for automatic correction of intensity nonuniformity in MRI data. *Medical Imaging, IEEE Transactions on* 17 (1), 87–97.
- Smith, K. D., Kallhoff, V., Zheng, H., Pautler, R. G., May 2007. In vivo axonal transport rates decrease in a mouse model of Alzheimer's disease. *NeuroImage* 35 (4), 1401–1408.
- Spring, S., Lerch, J. P., Henkelman, R. M., May 2007. Sexual dimorphism revealed in the structure of the mouse brain using three-dimensional magnetic resonance imaging. *NeuroImage* 35 (4), 1424–1433.

- Studholme, C., Cardenas, V., Blumenfeld, R., Schuff, N., Rosen, H. J., Miller, B., Weiner, M., April 2004. Deformation tensor morphometry of semantic dementia with quantitative validation. *NeuroImage* 21 (4), 1387–1398.
- Studholme, C., Cardenas, V., Maudsley, A., Weiner, M., August 2003. An intensity consistent filtering approach to the analysis of deformation tensor derived maps of brain shape. *NeuroImage* 19 (4), 1638–1649.
- Talairach, J., Tournoux, P., January 1988. *Co-Planar Stereotaxic Atlas of the Human Brain: 3-Dimensional Proportional System : An Approach to Cerebral Imaging*. Thieme Medical Publishers.
- Teipel, S. J., Bayer, W., Alexander, G. E., Zebuhr, Y., Teichberg, D., Kulic, L., Schapiro, M. B., Mller, H. J., Rapoport, S. I., Hampel, H., February 2002. Progression of corpus callosum atrophy in Alzheimer disease. *Arch Neurol* 59 (2), 243–248.
- Thal, D. R., Rb, U., Orantes, M., Braak, H., June 2002. Phases of A beta-deposition in the human brain and its relevance for the development of AD. *Neurology* 58 (12), 1791–1800.
- Thompson, M. D., Knee, K., Golden, C. J., March 1998. Olfaction in persons with Alzheimer’s disease. *Neuropsychol Rev* 8 (1), 11–23.
- Thompson, P. M., Hayashi, K. M., de Zubicaray, G., Janke, A. L., Rose, S. E., Semple, J., Herman, D., Hong, M. S., Dittmer, S. S., Doddrell, D. M., Toga, A. W., February 2003. Dynamics of gray matter loss in Alzheimer’s disease. *J. Neurosci.* 23 (3), 994–1005.
- Thompson, P. M., Hayashi, K. M., Dutton, R. A., Chiang, M. C., Leow, A. D., Sowell, E. R., De Zubicaray, G., Becker, J. T., Lopez, O. L., Aizenstein, H. J., Toga, A. W., February 2007. Tracking Alzheimer’s disease. *Ann N Y Acad Sci* 1097, 183–214.
- Thompson, P. M., Hayashi, K. M., Sowell, E. R., Gogtay, N., Giedd, J. N., Rapoport, J. L., de Zubicaray, G. I., Janke, A. L., Rose, S. E., Semple, J., Doddrell, D. M., Wang, Y., van Erp, T. G., Cannon, T. D., Toga, A. W., 2004. Mapping cortical change in Alzheimer’s disease, brain development, and schizophrenia. *NeuroImage* 23 Suppl 1.
- Thompson, P. M., Toga, A. W., September 1997. Detection, visualization and animation of abnormal anatomic structure with a deformable probabilistic brain atlas

- based on random vector field transformations. *Medical Image Analysis* 1 (4), 271–294.
- Tohka, J., Krestyannikov, E., Dinov, I. D., Graham, A. M., Shattuck, D. W., Ruotsalainen, U., Toga, A. W., May 2007. Genetic algorithms for finite mixture model based voxel classification in neuroimaging. *IEEE Trans Med Imaging* 26 (5), 696–711.
- Tohka, J., Zijdenbos, A., Evans, A., September 2004. Fast and robust parameter estimation for statistical partial volume models in brain MRI. *NeuroImage* 23 (1), 84–97.
- Trinchese, F., Liu, S., Battaglia, F., Walter, S., Mathews, P. M., Arancio, O., June 2004. Progressive age-related development of Alzheimer-like pathology in APP/PS1 mice. *Ann Neurol* 55 (6), 801–814.
- Verma, R., Mori, S., Shen, D., Yarowsky, P., Zhang, J., Davatzikos, C., May 2005. Spatiotemporal maturation patterns of murine brain quantified by diffusion tensor MRI and deformation-based morphometry. *Proc Natl Acad Sci USA* 102 (19), 6978–6983.
- Walhovd, K. B., Fjell, A. M., Reinvang, I., Lundervold, A., Dale, A. M., Eilertsen, D. E., Quinn, B. T., Salat, D., Makris, N., Fischl, B., October 2005. Effects of age on volumes of cortex, white matter and subcortical structures. *Neurobiol Aging* 26 (9), 1261–1270.
- Woods, R. P., December 1996. Modeling for intergroup comparisons of imaging data. *NeuroImage* 4 (3 Pt 3), S84–S94.
- Woods, R. P., Grafton, S. T., Watson, J. D., Sicotte, N. L., Mazziotta, J. C., 1998. Automated image registration: II. intersubject validation of linear and nonlinear models. *J Comput Assist Tomogr* 22 (1), 153–165.
- Xu, Y., Jack, C. R., O’Brien, P. C., Kokmen, E., Smith, G. E., Ivnik, R. J., Boeve, B. F., Tangalos, R. G., Petersen, R. C., May 2000. Usefulness of MRI measures of entorhinal cortex versus hippocampus in ad. *Neurology* 54 (9), 1760–1767.
- Zhang, C., McNeil, E., Dressler, L., Siman, R., October 2006. Long-lasting impairment in hippocampal neurogenesis associated with amyloid deposition in a knock-in mouse model of familial Alzheimer’s disease. *Exp Neurol*.

Zhang, J., Chen, Y.-B., Hardwick, M. J., Miller, M. I., Plachez, C., Richards, L. J., Yarowsky, P., van Zijl, P., Mori, S., February 2005. Magnetic resonance diffusion tensor microimaging reveals a role for Bcl-x in brain development and homeostasis. *J. Neurosci.* 25 (8), 1881–1888.

Zijdenbos, A. P., Dawant, B. M., Margolin, R. A., Palmer, A. C., 1994. Morphometric analysis of white matter lesions in MR images: method and validation. *Medical Imaging, IEEE Transactions on* 13 (4), 716–724.